FACULTY OF TECHNOLOGY

Direct reduction of chromite using the FFC Cambridge method

Saku Rytky

ENVIRONMENTAL ENGINEERING

Master's thesis

January 2023

TIIVISTELMÄ

Fossiilivapaiden metallintuotantoprosessien etsintä käy kuumana. FFC Cambridge - menetelmä on yksi vaihtoehto tällaiseksi CO_2-päästöjä pienentäväksi tai jopa kokonaan poistavaksi tuotantoprosessiksi. FFC Cambridge -menetelmää on käytetty jo useiden eri metallien pelkistykseen, mutta sitä ei ole vielä kokeiltu teräsnauhasintrattujen kromiittipellettien pelkistykseen. Tämän diplomityön tavoitteena oli tutkia FFC Cambridge -menetelmän soveltuvuutta Outokummun sintrattujen kromiittipellettien pelkistämiseen. Lisäksi työssä selvitettiin erilaisten inerttien elektrodien käyttömahdollisuuksia sekä pohdittiin, mitä haasteita FFC Cambridge -menetelmälle on mahdolliseen tuotannon ylös-skaalaukseen laboratoriokokeiden perusteella.

Työn kokeellisessa osassa esiteltiin käytetty koelaitteisto ja tutkittiin, mitä turvallisuusseikkoja kokeissa tulee ottaa huomioon. Lisäksi koesuunnitelmassa pohdittiin koeolosuhteiden mahdollisia rajoja ja selvitettiin kromiitin todellista koostumusta FESEM-EDS:n sekä XRF:n avulla. Työssä tehtiin koe 2,8 V jännitteellä, 900 °C lämpötilassa koeajan ollessa yksi tunti. Elektrolyyttinä toimi $CaCl_2$. Kokeen tulokset olivat toivoa herättäviä, sillä pieni määrä ferrokromia saatiin pelkistettyä onnistuneesti. Kokeet kuitenkin toivat esille useita eri haasteita seuraaville mahdollisille kokeille sekä mahdolliselle teolliseen mittakaavaan skaalaukselle: pellettien huono mekaaninen kestävyys, prosessin alhainen tehokkuus, hintavuus, tarve suunnitella ferrokromin valmistusprosessi uudelleen tätä prosessointimenetelmää varten ja elektrolyytin korroosiovaikutus.

Asiasanat: kromiitti, suorapelkistys, suolasulaelektrolyysi, FFC Cambridge

ABSTRACT

Direct reduction of chromite using the FFC Cambridge method

Saku Rytky

University of Oulu, Degree Programme of Environmental Engineering

Master's thesis 2023, 91 pp.

Supervisors at the university: Ville-Valtteri Visuri, Assoc. Prof., D.Sc. (Tech.) and Riku Mattila, M.Sc. (Tech.)

The guest for finding fossil-free alternatives to today's metal production processes goes strong. The FFC Cambridge process is one alternative to provide CO_2-lean or CO_2-free alternatives to conventional metal production processes. The FFC Cambridge process has been used to reduce a plethora of metal oxides via electrolysis, but the reduction of sintered chromite pellets from the industrial steel belt sintering process has not yet been experimented with. The main goal of this thesis was to study the applicability of the FFC Cambridge direct reduction method for reducing the sintered chromite pellets from Outokumpu Tornio works to ferrochrome. Also, the possibility of using inert anodes was reviewed together with discussion about the issues faced during the experiments that would pose challenges to the scale up of the process.

The experimental part of the study presents the experimental apparatus and the factors that needed to be evaluated before the experiments such as safety and experimental constraints. Additionally, the composition of chromite was analysed with FESEM-EDS and XRF. An experiment was conducted under voltage of 2.8 V, temperature of 900 °C and one hour electrolysis time in a $CaCl_2$ electrolyte. The results showed promise in the reduction of some chromite particles, but many challenges were identified for the future experiments and the possible scale-up of the process such as the low mechanical integrity of the pellets, low efficiency of the process, the expensiveness of the process, the need to reoptimize the ferrochromium manufacturing process, and the corrosive nature of the electrolyte.

Keywords: chromite, direct reduction, molten salt electrolysis, FFC Cambridge

ALKUSANAT

Oulu, 03.01.2023

Saku Rytky
Saku Rytky

TABLE OF CONTENTS

1 INTRODUCTION

Chromium and stainless steelmaking go hand-in-hand, since stainless steel contains at least 10.5 wt-% chromium by definition (Outokumpu 2022b). The chromium content of stainless steel varies between the different stainless steel grades; typically, the highest chromium content is found in duplex and austenitic grades, whereas lower amounts are found in martensitic and ferritic stainless steel grades (International Stainless Steel Forum 2022). Chromium is produced from chromite, which is in the mineral group of spinels, and is found in the earth's crust as $FeCr_2O_4$ ($FeO·Cr_2O_3$), but the quality of ore can vary from source to source (Habashi 1997 p. 1762-1766). Since magnesium and aluminum can substitute for iron and chromium in the crystal structure of chromite, another way is to give a general formula of $(Mg,Fe)(Cr,Al)_2O_4$ (King 2022). Silicon oxide is also present in the ore in smaller quantities together with other trace elements (Habashi 1997 p. 1762, Heikkilä et al. 2015). In Europe, the only chromite mine is located in Kemi (Outokumpu 2022a). The Kemi chromite has a Cr/Fe -ratio ranging from 0.81 to 1.87 (Habashi 1997 p. 1766).

Nowadays, ferrochrome is produced in electric energy utilizing submerged arc furnaces (SAF), which produce high CO_2 emissions and use high amounts of energy (Gynther & Kiuru 2020 p. 10). The manufacturing process of ferrochrome in the Outokumpu Tornio works is operated in closed submerged arc furnaces, which use coke as the main reducing agent (Outokumpu 2013 p. 24, Riekkola-Vanhanen 1999 p.13). Coke contributes to a large part of the CO_2 emission of ferrochrome manufacturing, but electricity use is the main culprit for the CO_2 emissions in the SAF process since the three Søderberg electrodes in the furnace can heat up to 3000 °C and consume huge amounts of energy (Riekkola-Vanhanen 1999 p. 1, p. 14, Hamuyuni et al. 2021). The specific numbers for electricity consumption can go up to 3 MWh per tonne of metal alloy (Hamuyuni et al. 2021).

The chromite ore Outokumpu Tornio works used in their process comes from the Kemi mine, which accounts for 1.1% of the earth's total chromite resources. With these reserves, the Outokumpu Kemi mine and Outokumpu ferrochrome works at Tornio together produce about 5% of the world's consumption of ferrochrome. (Erkkilä 2004, Outokumpu 2022a) The CO_2 emissions produced at Outokumpu Tornio works are by industry standards very low, since the worldsteel ISSF average is about 2.75 kg CO_2/kg

steel, while Outokumpu produces only about 1.6 kg CO_2/kg steel today (Outokumpu 2020). However, ferrochrome production alone uses up the same amount of energy compared to the rest of the stainless steel production process at Tornio works, thus it is important to find alternative means of production (Gynther & Kiuru 2020 p. 10).

As companies today are striving to become carbon-neutral, metal manufacturing companies have been driven to search for alternative methods for producing ferrochrome from chromite. Varying operating principles have been proposed ranging from electrolysis processes, via hydrogen plasma reduction to aluminothermic reduction. As for the electrolysis processes, both molten salt electrolysis (FFC Cambridge) and molten oxide electrolysis (MOE) have been proposed. It will also be interesting to see the changes in product composition compared to the SAF chromite reduction; the SAF ferrochrome from Outokumpu Tornio works contains about 54 wt-% chromium, 35 wt-% iron, 7 wt-% carbon, and 4 wt-% silicon (Metallinjalostajat 2014 p. 9).

The topic of this master's thesis is the direct reduction of chromite by the FFC Cambridge method under laboratory conditions. To this end, this thesis aims to find answers to the three following research questions:

1. can sintered chromite pellets from Outokumpu Tornio works be reduced using the FFC Cambridge method and under which process conditions?
2. are there other, inert, electrode alternatives to the CO_2 emission-producing graphite electrodes that have been used in the process in other studies?
3. what challenges to scaling up the process can be identified based on the experiment made in this thesis?

2 ELECTROLYTIC METHODS FOR THE DIRECT REDUCTION OF CHROMITE

Molten salt electrolysis has several different variants, of which the FFC Cambridge method is one. The basis of the molten salt methods is electrolysis in a molten salt electrolyte. The electrolytes are usually halide-based, of which chloride or fluoride electrolytes have been the most popular alternatives thus far. (Yan & Fray 2010) Molten oxide electrolysis is another alternative to the molten salt process, where the electrolyte is based on molten oxides. It is important to make a distinction between the different methods, even though at first it can be difficult due to similarities in the methods.

Other notable molten salt electrolysis processes are for example the Hall-Heroult process used for the manufacturing of aluminum, the Dow and I.G. Farben processes for the manufacturing of magnesium, and numerous different methods for the extraction of metals from waste materials (Yan & Fray 2010). Use of the molten salt electrolysis has a wide range from basic metallurgy to attempts of enabling life on the moon (Chen 2020). These methods can differ in many ways in terms of operation, but the basis of having molten salts in the electrolyte is true for all the methods (Yan & Fray 2010).

The alternative processing route provided by molten salt and oxide metallurgy is a promising way of offering CO_2-lean, or in the best-case scenario, CO_2-free alternatives to the traditional high-temperature metallurgy process alternatives. In this chapter, the operating principles of two different direct reduction methods are scrutinized: the molten salt electrolysis-based FFC Cambridge method and the molten oxide method. Both of these methods are very similar to each other in terms of operation, but in the last chapter 2.3, key differences between the two methods are analyzed. This chapter will focus more on the FFC Cambridge method, since it will be used in the experimental section of this thesis. Molten oxide electrolysis will also be reviewed in brief since it has been proposed as an alternative method for chromite reduction and is being experimented with by Aalto University during the TOCANEM project, which this thesis is a part of.

Both methods are based on electroreduction processes. Pure metals can be made with electrorefining or electrowinning. These are non-spontaneous electrolytic processes, where reduction happens at the negative cathode, and oxidation happens at the positive anode. In electrowinning, the source material for the metal is in the electrolyte as a

solution, and it can be reduced as a pure metal product and harvested from the cathode after electrolysis. In electrorefining, the aim is to obtain pure metal by electrolysis of the anode consisting of impurities and the product metal. The metal cations move from anode to cathode, while the impurities are left at the anode or suspended in the electrolyte, which ultimately provides nearly 100% purity metals. (Yan & Fray 2010, Scott 2019) The FFC Cambridge method differs from electrowinning by directly reducing the cathode material, meaning that cations do not need to migrate from the electrolyte to the cathode (Mohandas 2013). On the contrary, the molten oxide method has a quite similar principle of operation to electrowinning, as the metal cations need to migrate to the cathode from the electrolyte for reduction (Allanore 2014).

2.1 The FFC Cambridge method

The FFC Cambridge method is based on molten salt electrolysis, which can be operated at temperatures ranging from about 200 °C to 1000 °C (Yan & Fray 2010, Jiao et al. 2020). For the FFC Cambridge method itself, temperatures are usually in the 850 °C to 950 °C range (Mohandas 2013). This means these methods can be operated at a temperature lower than the melting point of the metals (Chen 2015). For example, titanium, chromium, vanadium, copper and iron have been successfully reduced at least in a laboratory-scale operation (Fenn et al. 2004). The FFC Cambridge method originated at the University of Cambridge from the scientists Derek Fray, Tom Farthing and George Chen, who applied the method for the reduction of TiO_2 (Fenn et al. 2004, Kvande & Vidal 2019). The method is not limited to deoxidizing metals, but it can also be utilized in the desulfurization of metals (Chen 2020).

The FFC Cambridge cell consists of the molten salt electrolyte, a cathode made of the metal oxide that is aimed to be reduced, an anode for oxygen ion reaction, a source of electricity, and a crucible, where the reaction occurs (Chen 2004). Argon gas together with a furnace that is sealed off from air is used to form the inert reaction atmosphere to prevent reoxidation of the metal cathode (Chen 2020).

The key reaction in this process is the reduction of the metal oxide in the cathode. Oxygen ions are dissolved, and the cathode only contains the reduced solid metal (Gordo et al. 2004). The cathodic reaction, applicable for all metal oxides, follows Eq. 1, where M represents the metal that is the product of reduction (Ge et al. 2015):

$$MO_x + 2\,xe \leftrightarrow M + xO^{2-} \tag{1}$$
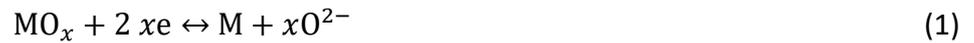
The anodic reaction is the other important reaction in the FFC Cambridge process. The oxygen ions travel to the anode and react forming CO_2 or oxygen, depending on if the anode material itself reacts with the ions (Hagen et al. 2007). The anodic reaction follows Eq. 2 if the anode is made of graphite and Eq. 3 if the anode is made of an inert material (Ge et al. 2015). Eq. 2 ultimately forms mostly CO_2 due to the reaction of CO with O_2, which then produces CO_2 (Chen 2020). The chemical reactions are shown in Figure 1 for a graphite anode cell.

$$xO^{2-} + C \leftrightarrow CO_x + 2xe \tag{2}$$

$$xO^{2-} \leftrightarrow \frac{x}{2}O_2 + 2xe \tag{3}$$
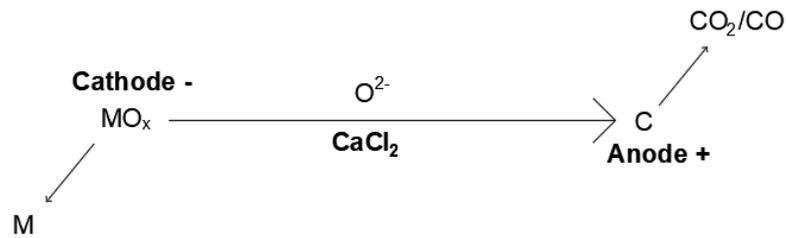
Figure 1. The chemical reactions in the FFC Cambridge process with a graphite anode.

The reactions mentioned above are simple, but the operation of the cell is complicated due to other reactions that occur in the electrolyte (Yan & Fray 2010). There has been debate on a calciothermic reduction process, where calcium metal is responsible for the reduction of the metal oxide. Some studies regarding the Ono-Suzuki process, one variation of the molten salt methods, (Suzuki et al. 2003) agree with this hypothesis in the case of reduction of TiO_2, but there has been scepticism for the validity of this mechanism in the case of reducing Cr_2O_3 (Schwandt & Fray 2007). Schwandt & Fray (2007) suggested that Cr_2O_3 would react with Ca^{2+} ions to chromium and $CaCr_2O_4$. The $CaCr_2O_4$ would then react to chromium and ions of Ca^{2+} and O^{2-}. According to the authors, this would mean that calciothermic reduction is not necessary in the FFC Cambridge process for the reduction of Cr_2O_3. Wang et al. (2020) summarized in their report about solid oxide membrane (SOM) assisted Cr_2O_3 reduction that the true mechanisms of the different reactions in the cell are still under debate, but also suggested

a similar reaction with Schwandt & Fray. The difference in this supposed mechanism is that Cr_2O_3 would react with Ca^{2+} ions to CrO and $CaCr_2O_4$ instead of chromium being directly reduced (Wang et al 2020). The $CaCr_2O_4$ would proceed to form CrO and CaO, which would ultimately form chromium with ions of calcium and oxygen (Wang et al 2020). Shurov et al. (2015) suggested that Ca^+ ions play an important role in the FFC Cambridge reduction process and questioned the presence of direct electrochemical reduction at least in case of metal oxides with low conductivity.

The basis of the FFC Cambridge process is the electrolysis of metal oxide pellets. These pellets are reduced to metallic pellets, which can be either used on their own in conventional metallurgy or be used to produce metal powders after crushing, milling and washing. (Chen et al. 2004) The whole process of converting a metal oxide pellet to either a powder or a metal pellet is summarized in Figure 2.
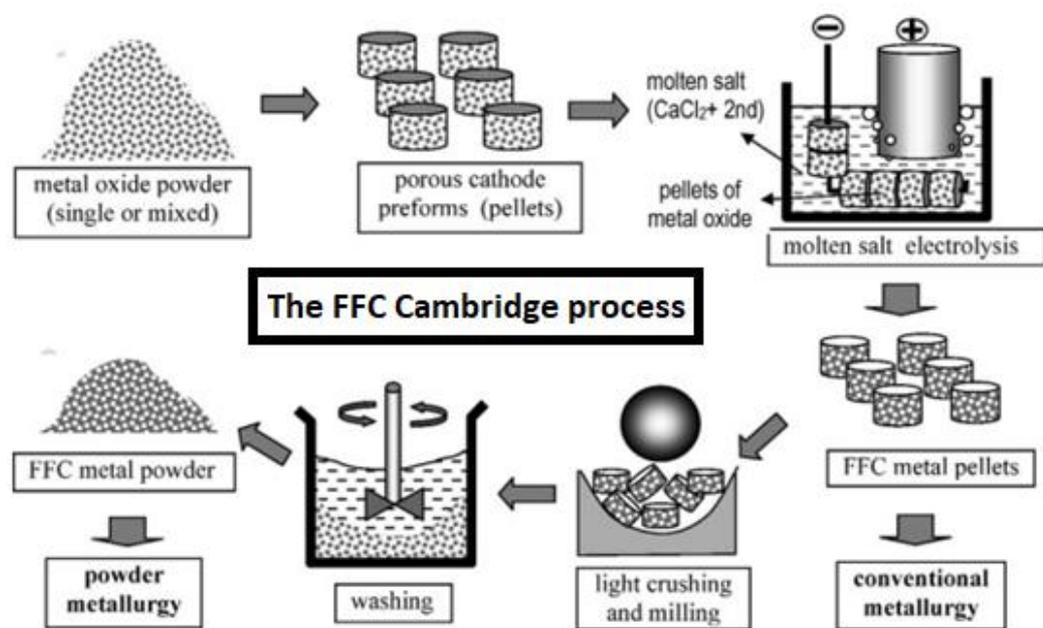
Figure 2. The FFC Cambridge process (modified from Chen et al. 2004).

2.1.1 Anodes

Hagen et al. (2007) have summarized the optimal anode with the following criteria in their patent:

1. the anode must be robust enough to withstand the operating temperature, thermal and mechanical shocks induced, and the corrosive environment of the cell,
2. the anode must not contaminate the cell or the cathode,

3. the anode must have good electric properties such as electric conductivity,

4. the anode should be affordable to be used in a profitable industrial process,

5. the anode should not react with the electrolyte, or the oxygen ions released from the cathode,

6. the use of the anode should not cause high vapor pressures in other components in the cell, and

7. the anode should be easily applicable to the cell.

In all the implementations published so far for Cr_2O_3 or chromite reduction (Chen et al. 2004, Gordo et al. 2004, Ge et al. 2015, Liu et al. 2017), graphite has been employed as the anode material. Carbon anodes, however, have some significant drawbacks if they are used due to their tendency to decompose and corrode. The unpreventable decomposition of the graphite anodes happens due to graphite reacting with oxygen ions to CO_2. This decomposition is accelerated by the CO_2 gas causing pressure differences in the pores of the anode after oxidation reactions have happened on the anode, ultimately causing larger particles of graphite to flake off the anode. (Chen 2020) The decomposition causes contamination of the electrolyte, which can cause a short-circuit, ultimately reducing the economic feasibility of the process through excessive current draw (Jiao & Fray 2010). Carbonates are also formed, which contaminate the cathode pellet in the cell and raise the current consumption even further (Jiao & Fray 2010, Hagen et al. 2007, Xiao & Wang 2013, Gordo et al. 2004). Figure 3 illustrates the carbon cycle in the electrolytic cell.

Figure 3. Carbon cycle inside the FFC Cambridge cell (modified from Chen 2020).

According to Chen (2020) and Hagen et al. (2007), to prevent contamination from the graphite anode, the electrolyte should be p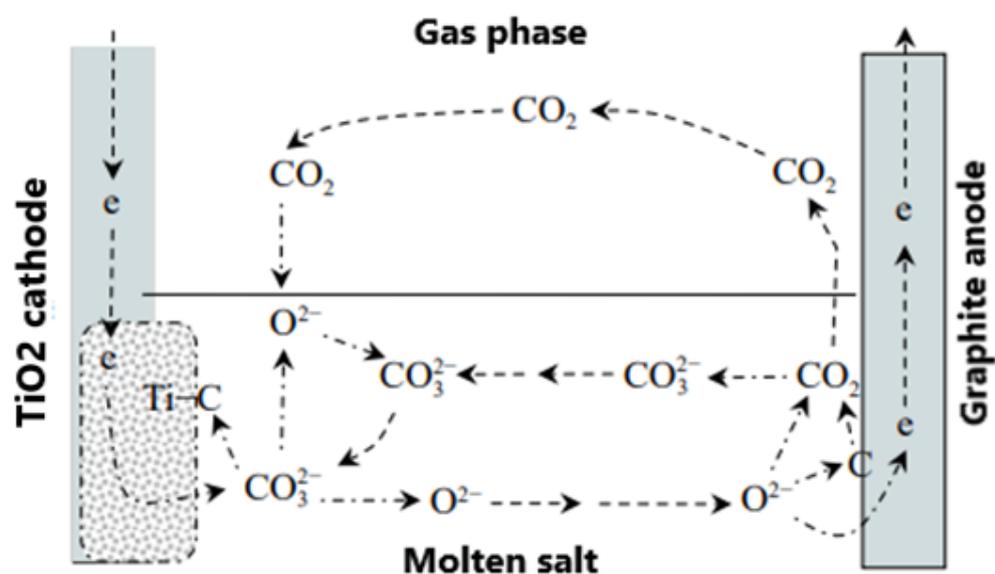ure $CaCl_2$ with a minimal concentration of oxygen ions and CaO, but this makes the ion travel in the cell less effective, poses risk for chloride ion formation, and requires a set temperature range between 900 °C and 1000 °C. Under these conditions, calcium carbonate is decomposed, but it is important to not exceed the temperature of 1000 °C to prevent the evaporation of chloride gases. (Chen 2020) Ion travel is reduced when operating with pure $CaCl_2$ due to the ability of CaO to enable the oxygen ion to travel from cathode to anode (Schwandt 2013). However, contradicting study by Liu et al. (2017) found that carbon contamination was minimized when using a 50-50 molar mixture of $NaCl$-$CaCl_2$ in their experiments. Another method for preventing carbon contamination is covering the cathode with an alumina tube with a hole for ion travel (Chen 2020). The salt in the electrolyte also influences the probability of decomposition of the anode, for example with LiCl-based electrolyte, the decomposition of graphite electrodes is faster than with a $CaCl_2$ electrolyte (Mohandas 2013).

Inert anodes are needed to reduce contamination and the risk of occurrence of short-circuiting but finding suitable materials for these anodes has been difficult (Wang & Xiao 2013). Proposed anodes have been the noble metals from iridium to platinum and alternatively with less noble metals, the respective oxides of the metals or different oxide-containing alloys (Wang & Xiao 2013). Alzamani et al. (2021) have also studied multi-metal inert anodes. Even with platinum-based anodes, which in theory should be inert, there has been a conclusion that there are still reactions happening that cause the platinum anode to erode (Mohandas 2013). With both $CaCl_2$ and LiCl-based electrolytes, the platinum anode is damaged due to the reaction of platinum with chloride ions (Mohandas 2013). Raising the concentration of CaO in $CaCl_2$, or another salt-dependent oxide, for example, Li_2O in LiCl, prevents the formation of Pt-Cl compounds, but the decomposition of the anodes will still proceed at a slow rate due to the reaction of platinum and oxide ions to Pt_3O_4, and Li^+, O^{2-} and Pt to Li_2PtO_3 (Mohandas 2013). These reactions have been reported in a review by Mohandas et al. (2013) in a LiCl electrolyte but would probably happen in a $CaCl_2$ electrolyte as well. However, recovery of the anode material partially is possible (Mohandas 2013), but due to the inflated costs of the inert material, this seems unfeasible, and it is necessary to continue looking for alternative inert anodes.

Other possible inert anode materials that have been studied in the FFC Cambridge process are $CaRuO_3$ anodes. Calcium ruthenate in $CaCl_2$ melts was studied by Jiao & Fray (2010) and they found that after 150-hour electrolysis, little decomposition was found at the anode. When the tests were done in a pure $CaCl_2$ electrolyte, corrosion was noticed, but with the addition of 1 wt-% of CaO in the electrolyte, the corrosion can be prevented, which follows the findings in Mohandas' (2013) review above. The overall corrosion rate with 1 wt-% of CaO was determined to be under $1.5 \cdot 10^{-3} \frac{g}{cm^2 \cdot h}$, which is very minimal. (Jiao & Fray 2010) The problem with $CaRuO_3$ anodes is their toxicity and prices on par with platinum metal (Wang & Xiao 2013, Umicore 2022). The cost of the anodes can be minimized by coating a $CaTiO_3$ anode with $CaRuO_3$ or mixing the two components to make an anode (Jiao & Fray 2010). Overall, $CaRuO_3$ seems to be a very promising material for inert anodes, and it would be interesting to see, whether there is a point in time, where major decomposition of the anode can be noticed.

SnO_2 anodes were used in the study by Barnett et al. (2009) to reduce Ta_2O_5. Both graphite and SnO_2 anodes were compared in the experiments. The study concluded that the current efficiency was better when using the inert anode compared to the graphite anode, as the current consumption with the SnO_2 anode is much lower in the current versus time -plots of the processes. Both inert and graphite anodes were noticed to decompose, but the inert anode weight loss was lower than that of the graphite anode. The overall reduction process was slower with the SnO_2 anode, which the authors deemed to be because of loss of conduction due to the formation of $CaSnO_3$. The use of SnO_2 anodes does not get rid of contamination of the cathode either, since there was Ta_3Sn_2 at the cathode after reduction. (Barnett et al. 2009)

$NiFe_2O_4$ inert anodes with intergranular nickel and copper were studied by Burheim & Haarberg (2010) in the reduction of Fe_2O_3. The reduction process was not completely successful, as copper was leached into the cathode and the cathode still contained high amounts of oxygen from 12 wt-% to 14 wt-%. Experiments were also made with a graphite anode. Compared to the graphite anode cell, the use of the inert anode was more efficient, because there was no carbon contamination. The use of graphite anodes was unsuccessful since carbon contamination was so severe that it ultimately stopped the reduction process due to blockage of the cathode pores. (Burheim & Haarberg 2010)

One of the most recent studies by Alzamani et al. (2021) used lanthanum as a doping agent in a NiFeCuAl alloy anode to increase the corrosion protection of the anode in the reduction of TiO_2. The mass percentages of lanthanum ranged from 0 to 0.0272 wt-%, the rest of the alloy contained 73.9 wt-% nickel, 10.8 wt-% iron, 9.9 wt-% copper, and 5.8 wt-% aluminum. The result of the study was that inducing lanthanum into the metal alloy anode improved corrosion resistance remarkably. Alzamani et al. (2021) noticed that the surface of the anode with the highest lanthanum content formed a stronger aluminum oxide surface on the anode due to lower porosity in comparison with the anode containing no lanthanum, increasing corrosion protection. Because the anode with the highest lanthanum content had the least corrosion among the other samples at the end of the 16-hour testing, it was selected for 120-hour electrolysis and the corrosion that was observed at the end was measured to have penetrated the anode at 70.69 μm deep from the surface. Lanthanum increases corrosion protection significantly since corrosion penetration measured from the surface is about 3.9 times higher in the shorter electrolysis experiments of the electrolyzed undoped sample compared to the longer electrolyzed doped sample. However, the product still contained some impurities such as $CaTiO_3$, TiO_6, and an unidentified compound. (Alzamani et al. 2021) These anodes could be great alternatives to be selected as inert anodes for the FFC Cambridge process due to reduced price compared to the $CaRuO_3$ anodes, since the content of the rare-earth element is very low. Hopefully, the impurities found by Alzamani et al. (2021) can be minimized by optimizing the electrolytic process and more data on the anode properties can be gathered. In Table 1, a list of anodes and their properties is presented.

Table 1. Properties of anodes used in the FFC Cambridge process.

Properties	Graphite	Pt	SnO_2	$CaRuO_3$	$NiFe_2O_4$	La-doped Ni-Fe-Cu-Al
Melting point (°C)	3850 [1]	1768.4 [10]	1630 [9]	>900 [6]	>920 [7]	>900 [8]
Boiling point (°C)	4250 [1]	3825 [10]	1800–1900 [9]	>900 [6]	>920 [7]	>900 [8]
Density (g/cm^3)	1.58–1.76 [2]	21.46 [10]	6.95 [9]	5.53 [11]	5.37 [13]	N/A
Resistance ($\mu\Omega m$)	4.2–8.5 [2]	N/A	N/A	Low at high temperature [6]	N/A	N/A
Price ($/kg)	2.99–3.94 [5]	29710 [3]	207.13 [4]	(Ru) 17720 [12]	N/A	N/A
Pros and cons	+ Cheap - Carbon contamination - Not inert	+ No carbon contamination - Expensive - Not inert	+ No carbon contamination + Cheap - Not inert - Ta_3Sn_2 contamination	+ Inert - Expensive if high amounts of Ru are used - Toxic	+ Cheap - Incomplete reduction - Copper leaching	+ Inert + Cheap

Notes: [1] Yvonne (2020), [2] Tokai carbon (2022), [3] MONEX (2022), [4] Merck (2022), [5] Stibbs & Pan (2022), [6] Jiao & Fray (2010), [7] Burheim & Haarberg (2010), [8] Alzamani et al. (2021), [9] The National Center for Biotechnology Information (2022a), [10] The National Center for Biotechnology Information (2022b), [11] Villars (2016a), [12] Umicore (2022), [13] Villars (2016b)

Separation of the cathodic and anodic reaction sections from one another in the electrolytic cell has been one alternative to reduce the degradation of the anodes. This method is called the solid oxide membrane (SOM) process. The operation principle is the same as in the FFC Cambridge process, the only difference being that there is a membrane separating the anode from the electrolyte. The method is based on the ability of the membrane to let through the oxygen ions towards the anode while preventing the corrosion that would normally happen at the anode due to contact with the electrolyte. A great advantage of this method is the ability to raise the cell voltage higher than the decomposition voltage of $CaCl_2$, enabling a much higher rate of reduction (Wang et al. 2020). For example, YSZ-zirconia membranes have been used, but there are problems with degradation of the membrane because the process must be run above 1000 °C to preserve high enough current density for the reduction process. (Martin et al. 2009)

2.1.2 Cathodes

The cathode should have adequate mechanical strength for enduring the electrolytic process, porosity for enhanced reactivity, and electric conductivity, thus high temperature and pressure sintered pellets of the metal oxides are used as cathodes (Schwandt 2013, Mohandas 2013).

A related topic regarding the properties of the anode is perovskitization. Ca_xTiO_y compounds are called perovskites. These ion blocking compounds accumulate into the pellet pores in the FFC process, thus the specific term that has been come up with is perovskitization. The adequate porosity and pore size are important factors to prevent this phenomenon, where calcium ions together with oxygen ions form compounds, generally representable as Ca_xTiO_y in TiO_2 reduction, that block ion travel from cathode to anode. In the case of Cr_2O_3, the formula that has been found in experiments has been $CaCr_xO_y$ (Ge et al. 2015). Perovskitization has been prevented in two ways:

- by first mixing CaO with TiO_2 in water to make $CaTiO_3$ perovskite cathode pellet and then electrolyzing the produced perovskite, or
- by inducing a compound, for example NH_4HCO_3, to the TiO_2 pellet that can be removed before electrolysis to increase the pore size to allow for oxygen ions to migrate away from the cathode before the migration channels inside the cathode become blocked.

The first method mentioned suffers from the need to raise the cell potential by about 0.23 V. (Jiang et al. 2006, Chen 2020)

Normally, solid metal oxide cathodes are used in the FFC Cambridge process. Deviating from the solid cathode approach, liquid metal cathodes have also been studied to be used in molten salt electroreduction. The electrochemical properties of the process and the purity of the product metal improve due to reduced contamination with oxygen but being able to reduce enough of the metal oxide has been proven difficult. This method has not yet been studied in the manufacturing of ferrochrome. (Jiao et al. 2020)

2.1.3 Electrolytes

The electrolyte in the FFC Cambridge process is salt-based. The main property of the electrolyte is the ability to contain the O^{2-} ions generated at the cathode, allowing them to move in the cell while not reacting with the cathode (Gordo et al. 2004). $CaCl_2$ has been the most used electrolyte for the FFC Cambridge method, but there have been studies with other molten salts, for example, NaCl, $BaCl_2$, LiCl, KCl, and their mixtures (Meurisse et al. 2022, Chen 2015, Wang & Xiao 2013, Gordo et al. 2004, Shurov et al. 2015, Liu et al. 2017). Fluorides are not typically used in the FFC Cambridge process due to their ability to dissolve the metal oxide cathode (Gordo et al. 2004).

$CaCl_2$ is used in ice removal from roads, and it is cheap and abundant, thus it is a great candidate in use for industrial processes as well (Espinha Marques et al. 2019, Suzuki et al. 2003) Addition of CaO to the $CaCl_2$ electrolyte lowers the risk of chloride ion formation, and renders most of the ion travel limitations from cathode to anode minute, allowing for shorter electrolysis times, but the CaO has also some negative effects to the overall cell due to its tendency to support above-discussed carbonate formation in graphite anode cells, increasing the current consumption, and enabling reaction of calcium with CO_2 to form carbon (Chen 2015, Mohandas 2013, Schwandt 2013).

Mixing of the salts has been reported to reduce the melting point of the electrolyte, improve electric conductivity, and lower the viscosity of the electrolyte, but in Cr_2O_3 reduction, the experiments by Gordo et al. (2004) showed that at the low temperatures of 600–750 °C, the reduction was not sufficient with $CaCl_2$-NaCl electrolyte thus meaning that ultimately the possibility of running electrolysis at lower temperatures for Cr_2O_3 reduction is not beneficial (Liu et al. 2017, Gordo et. al 2004). The negative effects may

be attributed to the reduced oxygen ion travel from the cathode to the anode and the reduced solubility of CaO in the electrolyte (Shurov et al. 2015). However, a later study by Liu et al. (2017) showed the benefits of using NaCl in the $CaCl_2$ molten salt, when the electrolysis temperature was risen to 800 °C due to the inhibited carbon reactions in the electrolyte due to lower temperature and decrease in solubility of oxygen ions in comparison with the $CaCl_2$ process. As the electrolyte salt is required to be molten, it means that the minimum temperature of operation is the melting point of the electrolyte salt. In Table 2, different properties of common electrolytes are presented.

Table 2. Properties of common electrolytes in the molten salt processes.

Salt electrolyte	Melting point (°C)	Boiling point (°C)	Vapor pressure at 900 °C (bar)	Applications
$CaCl_2$	772 [1]	1935 [1]	~0 [3]	Most common salt in the FFC Cambridge process [4]
NaCl	801 [1]:	1465 [1]	~0 [2]	Usually mixed with $CaCl_2$ [4]
$BaCl_2$	961 [1]:	1560 [1]	N/A	Usually mixed with $CaCl_2$ [4]
LiCl	610 [1]:	1383 [1]	~0 [3]	Nuclear waste applications for lowering the temperature of the process [5]
KCl	771 [1]:	N/A	~0 [2]	Usually mixed with $CaCl_2$ [4]
NaCl-$CaCl_2$	500 [1]	N/A	N/A	Reduces carbon contamination in Cr_2O_3 reduction, improves current efficiency [6]

Notes: [1] Rumble (2022), [2] Li et al. (2014), [3] Ding et al. (2018), [4] Meurisse et al. (2022), [5] Mohandas (2013), [6] Liu et al. (2017)

2.1.4 Previous studies of the FFC Cambridge process regarding chromite and its components

Cr_2O_3, Fe_2O_3 and chromite ore reduction have been studied in the past by Chen & Fray (2006), Chen et al. (2004), Ge et al. (2015), Guoming et al. (2009), Liu et al. (2017), Wang et al. (2020) and Gordo et al. (2004). Studies range from morphological studies to variations of different operating variables.

The study by Ge et al. (2015) focused on the three important aspects of chromite reduction: they reduced pure Cr_2O_3, a mixture of Cr_2O_3 and Fe_2O_3 and most importantly, chromite ore. Reduction with all three was successful in reducing the oxides to metal form, but there were some impurities of other metal oxides in small quantities in the ore reduction. They used a voltage ranging from 2.8 to 3.0 V and a temperature of 900 °C was found optimal in their experiments. They used sintered Cr_2O_3, Fe_2O_3, and chromite disks, and obtained the best results with the pellets sintered at 1150 °C for all three tests. The authors deemed this to be due to the better oxygen diffusion of the smaller particles in comparison with the 1350 °C sintered ones, and better homogenous cubic structure compared to 950 °C sintered pellets.

An important finding in the study for Cr_2O_3 reduction was that during the first stages of electrolysis, calcium chromate is formed, and if the electrolysis is prolonged, chromium contaminated with carbon is formed. 4-hour electrolysis of Cr_2O_3 was deemed optimal, and for the mixture of Cr_2O_3 and Fe_2O_3, 10 hours was required for complete reduction. The iron oxides are reduced at the initial stages of electrolysis, followed by a longer reduction time of Cr_2O_3. The reduction was reported to start from the electrode-pellet contact area, proceeding at a rapid rate to the inside of the pellet in the case of surface reduction and at a slow rate towards the surface at the inside of the electrode-pellet contact area.

Gordo et al.'s (2004) study about Cr_2O_3 and altering the electrolysis variables had similar findings that the sintering temperature should be about 1000–1100 °C, and the cell voltage should be 2.7–2.8 V. The sintering temperature affects the particle size of the Cr_2O_3 pellets, and the optimal particle size was deemed to be under 5 micrometers when considering the reduction of the pellets. Including NaCl into the $CaCl_2$ electrolyte did not benefit the process, since running the electrolysis at lower temperatures of 600–750 °C

did not facilitate the reduction of Cr_2O_3. The complete reduction could be achieved in 4 to 6 hours, just like in Ge et al.'s (2015) study. (Gordo et al. 2004)

Chen & Fray (2006) investigated the morphological side of Cr_2O_3 reduction. The main finding was that chromium metal tends to form cubic particles from nodular ones as the electrolysis progresses, because they have less affinity to oxygen. In comparison, titanium forms nodular particles, as it has a higher affinity to oxygen. The reason for this is that the oxygen compounds can interrupt the growth of cubical particles. (Chen & Fray 2006)

Chen et al. (2004) focused on Cr_2O_3, and they used constant operating conditions with no variation. The study tested different electrolysis durations together with different positionings of the cathodes in the cell. Also, the effects of different sintering techniques were investigated. A relatively full reduction was achieved at 950 °C, 2.7–2.8 V cell potential and electrolysis duration of 4–6 hours; after the six-hour electrolysis the measured oxygen content was 0.186 wt-%. Results showed that the reduction starts at the surface next to the electrode contact point of the pellet, proceeding to the inside of the metal oxide following the phase interlinks between the oxide, metal, and the electrolyte, which goes along with the findings of Ge et al. (2015). Calcium chromates ($CaO \cdot Cr_2O_3$) were also detected in the early stage of electrolysis and similar conclusions regarding the sintering temperature of the pellets were concluded in the studies by Ge et al. (2015) and Gordo et al. (2004) mentioned above. (Chen et al. 2004)

Guoming et al. (2009) studied Fe_2O_3 reduction and found that the reaction does not directly proceed from Fe_2O_3 to Fe. Rather, the reduction starts by forming FeO as an intermediate compound that is finally reduced to Fe. Similar findings have been reported for the reduction of Cr_2O_3 (Wang et al. 2020). Oxygen ions are released at the cathode, ultimately forming oxygen gas, but the escape of oxygen might not take place if graphite anodes were used. The anode employed was not specified in the study. The reduction was also reported to have proceeded at a rapid rate, which goes along well with above-mentioned studies. Also, one interesting note the authors made was that the cell voltage and electrolysis time effects also the structure of the reduced Fe product: preferred homogeneously sized cubic particles are formed at low voltages, but when increasing the voltage, the particles are nodular and have a larger variety in their size. As for the electrolysis time, the main effect is on the size of the product particles: the longer time for electrolysis, the larger the particles that are formed. (Guoming et al. 2009)

Liu et al. (2017) studied the reduction of Cr_2O_3 with a mixture 50-50 molar mixture of $CaCl_2$ and NaCl. The study found optimal conditions for Cr_2O_3 reduction to be at "3.2 V, 800 °C, 1100 °C sintering temperature, and 8-hour electrolysis time". The lower temperature and the inhibited solubility of oxygen ions to the electrolyte, which ultimately reduces carbon contamination, was reported as an advantage of the reduction process with $CaCl_2$–NaCl. One benefit of adding NaCl to the molten salt was also increased current efficiency. The downside of the process is the higher oxygen content of the product, because the $CaCl_2$ electrolysis can produce products with an oxygen content of 0.2 wt%, compared to the $CaCl_2$–NaCl electrolysis 0.5 wt-%. The study also found differences in the morphology of the products, as there were no cubic chromium particles formed. The products were always nodular in morphology. (Liu et al. 2017)

The SOM process has also been studied in the reduction of Cr_2O_3 by Wang et al. (2020). The use of the membrane allows for high voltages to be applied to the cell, considerably lowering the electrolysis time needed. The 3.5 V voltage used by the authors allowed for 100% reduction of Cr to occur on the surface in about three hours, but the inside of the pellet still contained about 5 wt-% oxygen after electrolysis, but no calcium compounds were detected. Sintering temperature was found to be very important, since the pellets sintered at 1100–1150 °C had no oxygen in them after electrolysis, but when the sintering temperature rose to 1200, the products contained 0.48 wt-% oxygen and in the pellets sintered at 1300, the oxygen content dramatically rose to 7.44 wt-%. (Wang et al. 2020)

The findings regarding used and optimal values of each study are summarized in the Table 3 below.

Table 3. Characteristics of previous experiments in the reduction of chromium oxide, iron oxide, and chromite.

Characteristic	Study					
	Ge et al. (2015)	Gordo et al. (2004)	Chen et al. (2004)	Guoming et al. (2009)	Liu et al. (2017)	Wang et al. (2020)
Was the relationship between different variables studied to find the optimum?	Yes	Yes	No	No	Yes	Yes
Cathode material	Chromite	Cr_2O_3	Cr_2O_3	Fe_2O_3	Cr_2O_3	Cr_2O_3
Temperature (°C)	900	850–950	950	800	800	1150
Voltage (V)	2.8 V	2.7–2.8	2.8	1.0–3.2	3.2	3.5
Electrolysis time (h)	8	4–6	4–6	2–20	8	2
Sintering temperature (°C)	1150	1000–1100	1000	800	1100	1100–1150
Sintering pressure (MPa)	10	172	154	7	170	4
Molten salt	$CaCl_2$	$CaCl_2$	$CaCl_2$	$CaCl_2$	$CaCl_2$–NaCl (50-50 molar mixture)	$CaCl_2$

2.2 Molten oxide electrolysis method

The molten oxide method employs an oxide electrolyte, and it is used for the direct reduction of metals, for example iron (Wiencke et al. 2018). The temperature of the process is similar to the high temperatures used in today's metalmaking (Wiencke et al. 2018). In ironmaking, several oxygen-based electrolytes have been used, for example, a mixture of SiO_2, MgO, CaO and Al_2O_3 together with Fe_3O_4, which the process reduces at the cathode (Esmaily et al. 2020). The product is molten metal, which can then be sent through a casting process (Esmaily et al. 2020).

In Figure 4, a representation of the molten oxide method for the reduction of metals is shown. The method's basis is the idea of reducing the metal-oxide from the electrolyte as pure metal at the cathode (Allanore 2014). The electrolyte consists of different oxides and the metal oxide that is aimed to be reduced, for example, Fe_3O_4 (Esmaily et al. 2020).
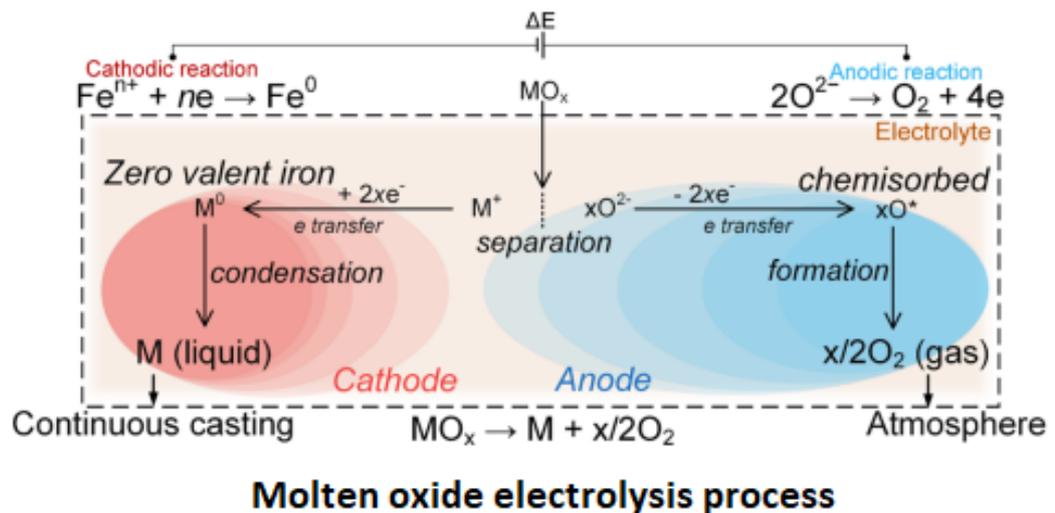
Figure 4. Molten oxide electrolysis of iron (modified from Esmaily et al. 2020).

Graphite rods have been used as anodes in the molten oxide cells similarly to the FFC process, but there have also been several experiments in finding a suitable, inert, anode material, for example ferrochrome alloy, since there are similar drawbacks of using graphite anodes, just like in the FFC process (Esmaily et al. 2020, Allanore 2014). Overall, many studies employ inert anodes, for example platinum (Wiencke et al. 2018), Iridium (Kim et al. 2019), and Cr-Fe alloy (Esmaily et al. 2020).

The disadvantage of this method is high energy use due to higher operating temperatures. The refractory materials of the electrolytic cell are subjected to more wear at higher temperatures and the heat losses cause excess energy requirements. (Allanore 2014, Wang & Xiao 2013)

2.3 Comparison of the two methods

The most obvious difference between the two methods is the temperature difference. FFC Cambridge is classified as a moderate-temperature process, while the molten oxide method is employed in the high temperatures steel-making industry used in the past. For example, molten oxide electrolysis of iron is carried out at temperatures of about, at the melting temperatures of 1400–1600 °C (Esmaily et al. 2020), while the molten salt electrolysis of iron is done in temperatures of 800–900 °C, under the melting point of the metals (Guoming et al. 2009). Higher temperatures used in the molten oxide electrolysis are more demanding for the materials in the cell, but the nature of the electrolyte is also demanding in terms of corrosion for the FFC Cambridge process (Wang & Xiao 2013).

The overall ion migration paths of the processes also differ, since in the FFC Cambridge process, the cations of the product metal do not need to migrate to the cathode from the electrolyte like in the molten oxide process (Fenn et al. 2004, Zhang et al. 2021). The product metal in the FFC Cambridge method is reduced as a solid product, while in the molten oxide method, the product is usually extracted in liquid form, although extraction as solid is also possible (Chen 2015, Allanore 2014).

The electrolytes differ in the two processes. The molten oxide method has oxides in the electrolyte, while the FFC Cambridge method uses molten salts. The conductive nature of the salt electrolytes at high temperatures gives them an advantage over molten oxide electrolysis due to their better electrochemical properties (Jiao et al. 2020). Supporting this claim, one of the challenges of the molten oxide method is the adequate conductivity of the electrolyte and creating optimal electrolytes due to the complexness of molten oxide electrolyte thermodynamics (Allanore 2014).

An advantage of the molten oxide method is that the electrolyte does not contain halides that can evaporate and cause air pollution. For example, in the FFC Cambridge process, the $CaCl_2$ electrolyte can evaporate as hazardous Cl_2 gases (Kvande & Vidal 2019).

Another downside of the halide-based electrolyte is its tendency to corrode materials (Wang & Xiao 2013). In Table 4, key differences and similarities between the FFC Cambridge and molten oxide electrolysis processes from different sources are listed.

Table 4. Comparison of the FFC Cambridge and molten oxide electrolysis processes.

Properties	FFC Cambridge						MOE			
Electrolyte	Salt-based [10]						Oxide-based [11]			
Cathode	Reducible metal oxide [10]						Liquid Fe [1]	Pt-Rh [2]	Mo [3]	
Anode	Graphite [4]	Pt [5]	CaRuO$_3$ [6]	SnO$_2$ [7]	LaNiFeCuAl [12]	NiFe$_2$O$_4$ [13]	Graphite [1]	Ir [3]	CrFe [8]	Pt [2]
Product metal and temperature (°C)	Fe 800 [7]		Cr 900 [4]		Ti 950 [9]	Fe-Cr 900 [4]	Fe 1565-1600 [8]		Ti-Fe 1600 [1]	
Reducible materials	Metal oxides and sulfides attached to the cathode [14]						Metal oxides in the electrolyte [11]			
Manufacturing of alloys	Possible [4], [10]						Possible [1]			

Notes: [1] Jiao et al. (2018), [2] Wiencke et al. (2018), [3] Kim et al. (2019), [4] Ge et al. (2015), [5] Mohandas (2013), [6] Jiao & Fray (2010), [7] Barnett et al. (2009), [8] Esmaily et al. (2020), [9] Fray et al. (2000), [10] Fenn et al. (2004), [11] Allanore (2014), [12] Alzamani et al. (2021), [13] Burheim & Haarberg (2010), [14] Chen (2020)

3 DESIGN OF EXPERIMENT

3.1 Experimental boundaries

The experimental boundaries for the experiments are set by the melting point and decomposition voltages of the salts used. For $CaCl_2$, the maximum voltage that can be used is approximately 3.2 V, since beyond that, the salt starts to decompose into Ca and $Cl_2(g)$ (see Figure 5). The minimum voltage of operation is the decomposition voltage of Cr_2O_3, which is 0.412 V for the graphite electrodes, but the true minimum would probably be the dissolution voltage of CaO to O_2 or CO_x, which in standard cell potentials are about 2.65 V for inert anodes and 1.54 V for carbon anodes due to the possibility of calciothermic reduction reaction and the enhanced oxygen ion travel enabled by CaO (see Figure 5). The minimum temperature is the melting point of $CaCl_2$, which was mentioned previously to be 772 °C. Optimal temperature ranges in previous chromite reduction tests have been proven to be around the 900–950 °C range. At these temperatures, $CaCO_3$ formation can also be prevented if the reduction reaction is complete (Gordo et al. 2004). Temperatures lower than 900 °C have less efficiency of reduction. Use of higher temperatures poses many risks, as Ge et al. (2015) found that already at 1000 °C and a voltage of 3.0 V, $CaCl_2$ starts to evaporate, and the graphite anodes are subjected to high wear (Ge et al. 2015).

3.2 Preparation of the experiments

Our preparations for the experimental section consist of cell voltage calculations and taking into consideration the safety concerns for the experiments.

3.2.1 Cell voltages

Voltages used in the cell need to be high enough to reduce the metal oxide, but low enough to avoid the decomposition of $CaCl_2$ (Gordo et al. 2004). The appropriate cell potential can be calculated with the Nernst equation (Kvande & Vidal 2019):

$$E_{cell} = E_{cell}^0 - \frac{RT}{zF} \ln Q, \tag{4}$$

where E_{cell}^0 is the standard cell potential, R is the universal gas constant, T is the temperature, z is the is the number of electrons transferred in the cell reaction, F is the Faraday constant, and Q is the reaction quotient. The standard cell potential can be calculated with the following equation:

$$E_{\text{cell}}^0 = \frac{\Delta G^0}{zF},$$ (5)

where ΔG^0 is the change in standard Gibbs free energy. The reaction quotient can be calculated with the following equation:

$$Q = \prod_i a_i^{v_i},$$ (6)

where a is the activity and v is the stoichiometric coefficient, which has negative values for reactants and positive values for reaction products.

The different reactions in the cell have their own voltage areas at different temperatures. Figure 5 and Figure 6 represent the standard cell voltages for the different reactions in the electrolyte and the standard cell voltages for the reduction of the components of chromite, respectively. These standard cell potentials are calculated with Eq. 5. Figure 7 represents the estimations of voltage ranges assuming a CO/CO_2 partial pressure ratio of 1000 and an oxygen partial pressure of $8.4 \cdot 10^{-23}$ atm. Eq. 4 and Eq. 6 were used in calculating the actual cell potentials after calculating oxygen partial pressure with Eq. 7:

$$p_{O_2} = \frac{1}{K \cdot \frac{p_{CO}^2}{p_{CO_2}^2}},$$ (7)

where K is the equilibrium constant and p denotes the partial pressure.
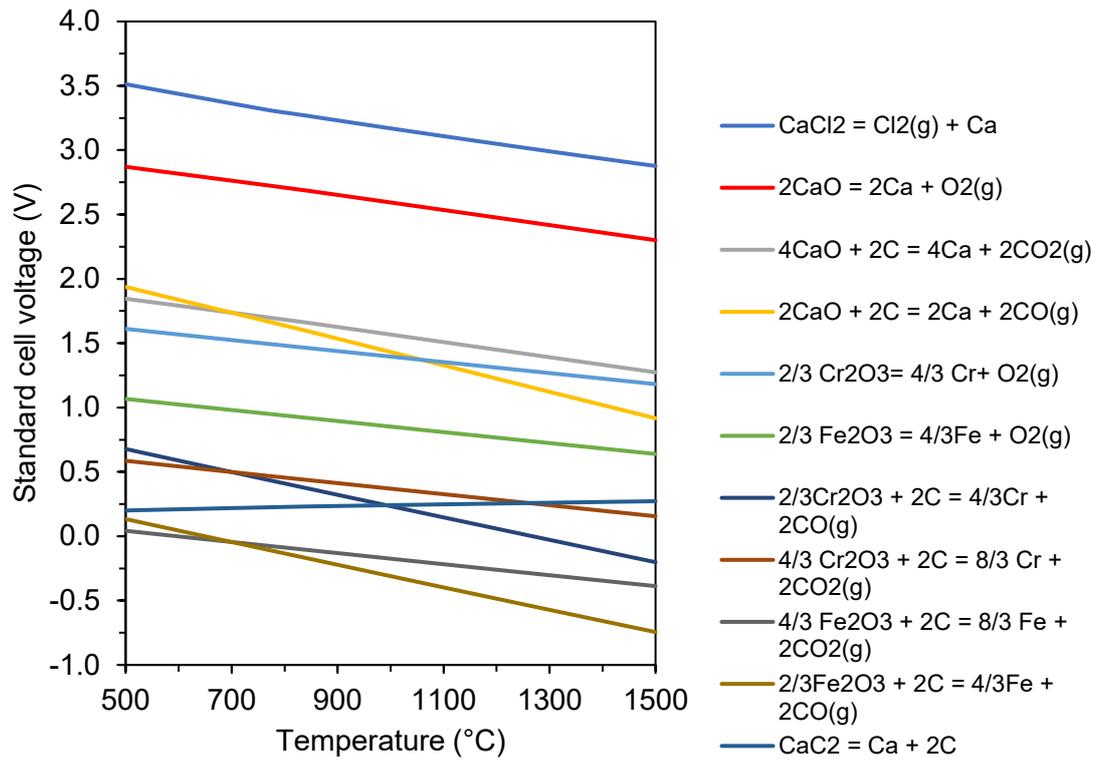
Figure 5. Calculated standard cell potentials of different reactions in the cell.

In Figure 6 standard cell potentials for reduction of different components of chromite is calculated.
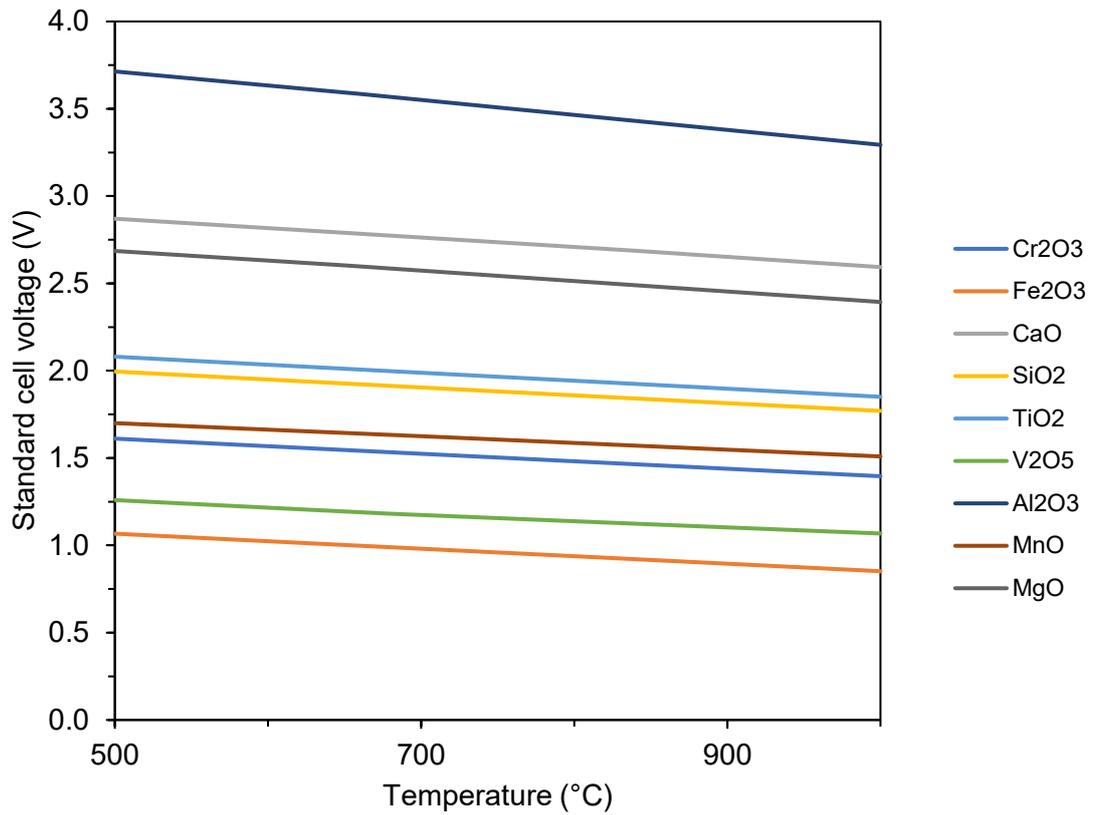
Figure 6. Calculated standard cell potentials for chromite components.

Figure 6 shows that vanadium can form at the reduction voltages of Cr_2O_3. MnO's reduction voltage is slightly higher than Cr_2O_3's, but it would require a very precise voltage control to not reduce the MnO. At 900 °C, the reduction voltage is 1.44 V for Cr_2O_3 and 1.55 V for MnO. Thus, the experimental apparatus should be fitted with a reference electrode to get an accurate reading of the voltage depending on the product quality requirements.
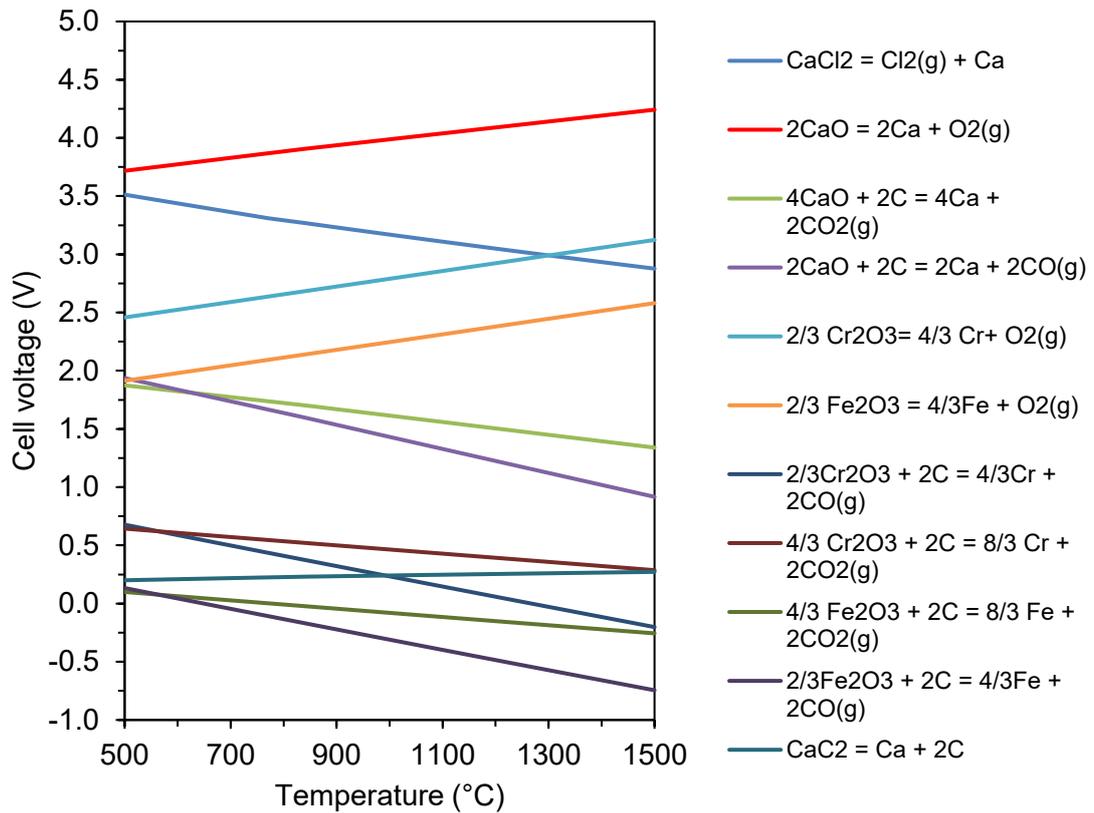
Figure 7. Calculated cell potentials of different reactions in the cell assuming $p_{CO}/p_{CO2}=1000$ and $p_{O2}=8.4\cdot10^{-23}$ atm.

The standard cell potentials for metal reduction with graphite anodes are lower than with inert anodes, but due to reactions of the carbon in the electrolyte, the overpotential is higher than with inert anodes and this advantage of the carbon anodes is smaller in actual cell potentials (Mohandas 2011).

Other studies have estimated the true cell potentials by calculating the standard cell potential and analyzing the possible overvoltage, but in this study, we have tried to calculate the cell voltages by calculating the cell potentials according to Eq 4. The partial pressures of oxygen have been calculated with thermodynamic data for the reaction of CO and O_2 to CO_2 from the HSC 9 program at the experimental temperature range using Eq. 7.

Chen (2020) has suggested that the partial pressure of CO_2 would be much higher than the partial pressure of CO and O_2. According to the results of the voltage calculations of this work, it would mean that the cell potential of $CaCl_2$ dissolution would be higher than the dissolution potential of the CaO reduction, meaning CaO dissolution without decomposition of $CaCl_2$ would be possible with inert anodes as well. With the CO/CO_2

partial pressure ratio of 1/1000, the potentials for both dissolutions would be almost equal. When the ratio is lowered further to 1/10000 and 1/100000, the dissolution potential of $CaCl_2$ at 900 °C is about 0.1 V and 0.2 V higher than the dissolution potential of CaO to oxygen and calcium, respectively. Figures 8, 9, and 10 show these potential changes.

Figure 8. Calculated cell potentials of different reactions in the cell at the temperature range of 500–1500 °C assuming $p_{CO}/p_{CO2}=1/1000$ and $p_{O2}=8.4 \cdot 10^{-11}$ atm.

Figure 9. Calculated cell potentials of different reactions in the cell at the temperature range of 500–1500 °C assuming $p_{CO}/p_{CO2}=1/10000$ and $p_{O2}=8.4·10^{-9}$ atm.
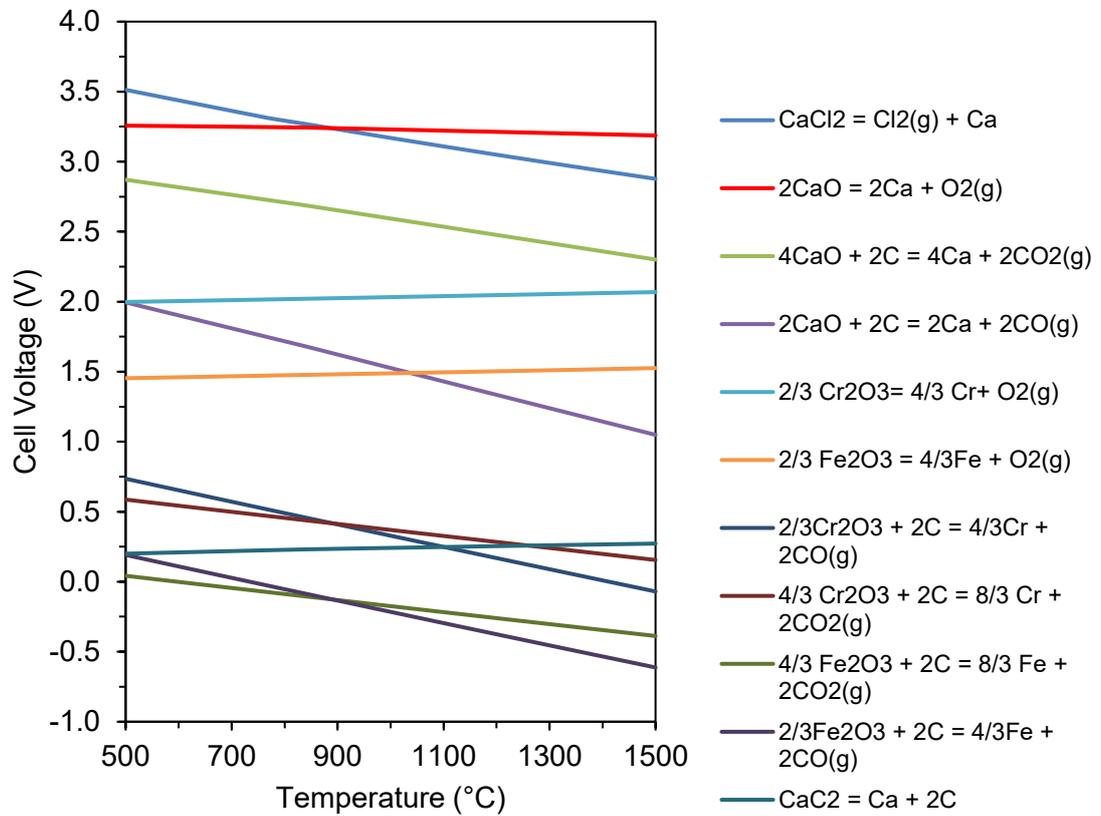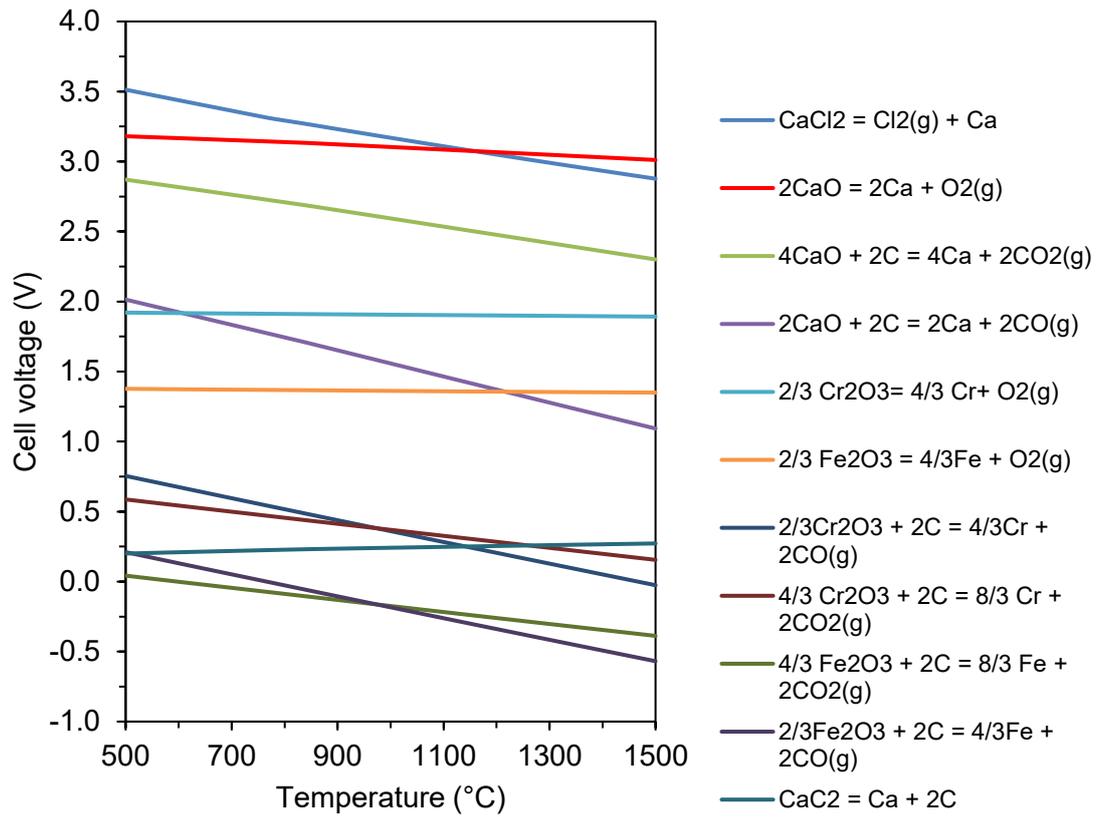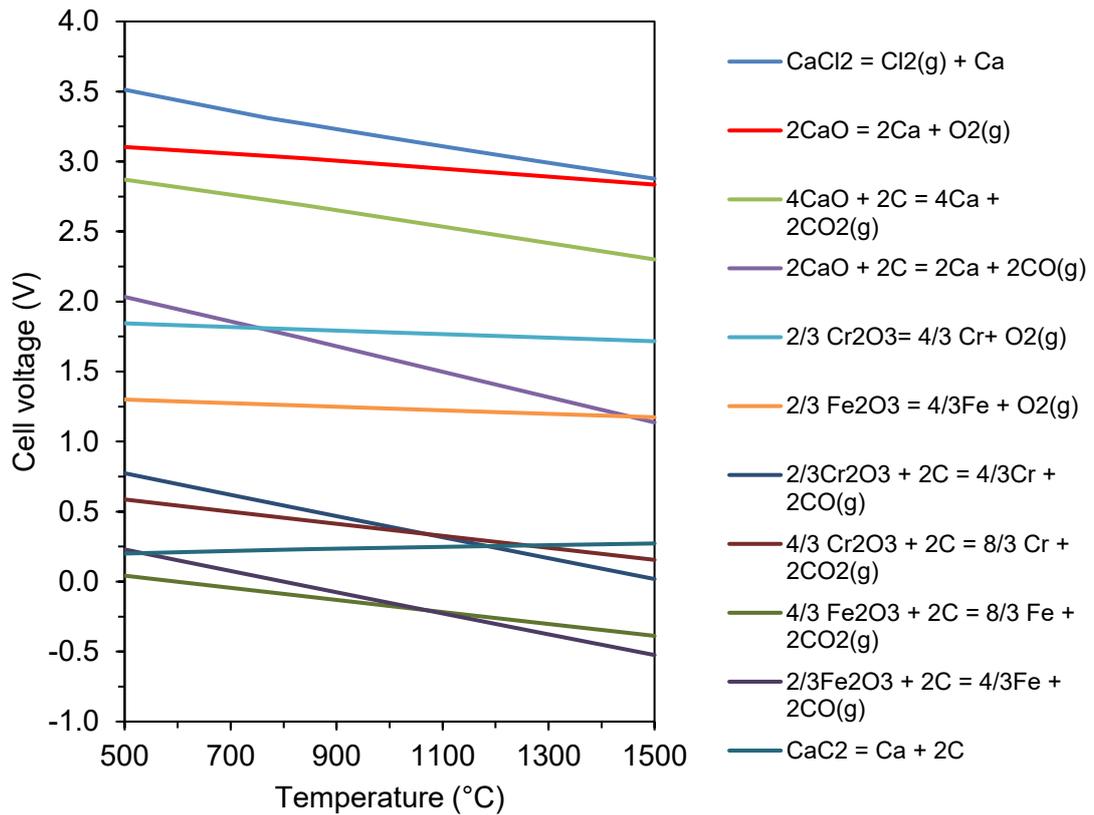
Figure 10. Calculated cell potentials of different reactions in the cell at the temperature range of 500–1500 °C assuming $p_{CO}/p_{CO2}=1/100000$ and $p_{O2}=8.4\cdot10^{-7}$ atm.

The true partial pressure ratios are however very difficult to estimate, as there is high variation in the partial pressure of CO_2 during the electrolysis and in different parts of the system (Schwandt & Fray 2007). What we can gather from these calculations is that optimally, the p_{CO}/p_{CO2} -ratio should be under 1/10000 to be able to have a gap between the dissolution potential of $CaCl_2$ and CaO. The partial pressure of Cl_2 is also assumed to be 1, but if the partial pressure is lower, the cell potential will rise to make the control of cell potential in the system easier. However, the dissolution potential of CaO to calcium, CO_2, and CO are always lower than the dissolution potential of $CaCl_2$, which would mean that this does not have as much relevance when using graphite anodes.

3.2.2 Safety concerns of the experiments

$CaCl_2$ as an electrolyte forms safety concerns in the form of evaporation of Cl_2 -gases. Cl_2 gas itself is toxic to humans, and the dangers are multiplied by the risk of Cl_2 explosively reacting with hydrocarbons or forming toxic and corrosive HCl with hydrogen from water, thus preventing the formation of chloride gas and preheating the experimental apparatus before use are necessary (Työterveyslaitos 2022). Preventative

measures are done by using a sealed reactor to prevent hydrolysis and elevated partial pressure of oxygen in the reactor. Calculations were performed to find out the maximum partial pressure of oxygen at 750–1000 °C to prevent formation of 0.5 ppm Cl_2 gas, which is the known threshold for toxicity in humans (Työterveyslaitos 2022). HSC 9 was used to determine the partial pressure of oxygen for Eq. 8.

$$2 \ CaCl_2 + O_2 \leftrightarrow 2 \ CaO + 2 \ Cl_2 \tag{8}$$

The partial pressure of oxygen can be calculated with the following equation:

$$p_{O_2} = \frac{a_{CaO}{}^2 \cdot p_{Cl_2}{}^2}{a_{CaCl_2}{}^2 \cdot K} \tag{9}$$

where a_{CaO} and a_{CaCl_2} are assumed to be 1 for pure substances. K is calculated with HSC 9 reaction equation module for the temperature range of 750–1000 °C. p_{Cl_2} is taken as $5 \cdot 10^{-7}$ atm at all temperatures. According to our calculations for the experimental temperature range, the partial pressure of oxygen should be below $1.037 \cdot 10^{-1}$ atm at the approximate melting point of $CaCl_2$, and below $2.232 \cdot 10^{-3}$ atm at the operating temperature of 900 °C. Figure 11 shows the calculated partial pressure of oxygen versus temperature.
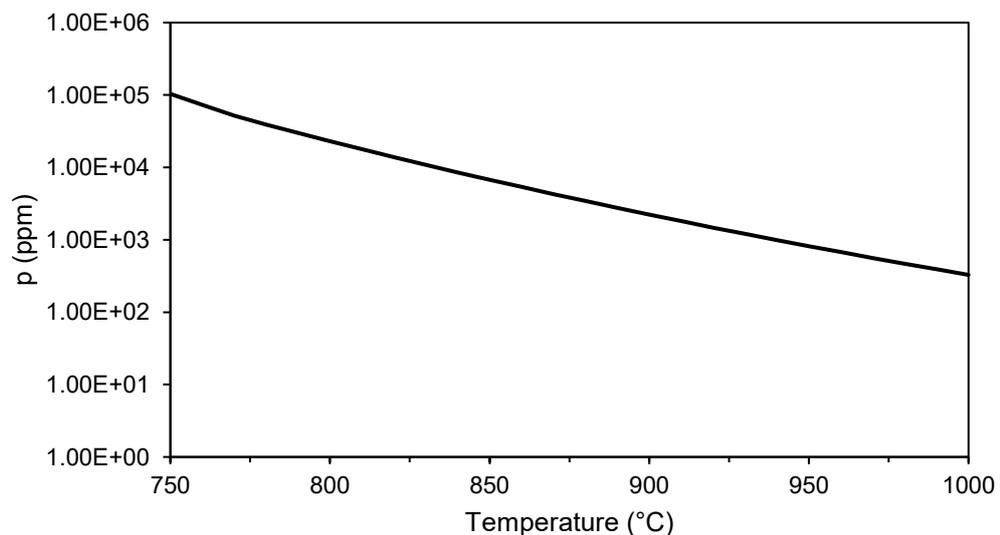

Figure 11. Partial pressure of oxygen versus temperature at 0.5 ppm Cl_2.

Hydrocarbons need to be separated from the experimental environment due to the possible explosive reaction with Cl_2. Coke consists mostly of hydrocarbons; thus, it

should not be present in the cell for safety reasons. Coke is mixed into the sintered pellets during the Outokumpu pelletizing-sintering process, but due to the high temperature of 1350 °C in the process, the hydrocarbons are combusted, and the electrolysis process will be safe from coke in the pellets (Riekkola-Vanhanen 1999 p. 23). The only way hydrocarbons can be formed is from outside contamination, thus the cell will be sealed from hydrocarbon contamination, and the process can be deemed safe.

3.3 Chromite ore pelletizing-sintering process

Chromite pellets used in this study are produced by the Outokumpu pelletizing-sintering process. The first stage of the process is pelletizing, where bentonite and process dust is mixed with the fine chromite ore. The pelletizing drum produces pellets with a diameter of 12–13 mm, which are sent to the sintering steel belt furnace. The sintering removes moisture from the pellets and coke is used to provide fuel for melting the silicates to increase the sintered pellets' mechanical strength. Sintering also increases the porosity of the pellets, which is beneficial not only for the submerged arc furnace process, but for the FFC Cambridge process as well. The temperature in the sintering furnace rises to approximately 1350 °C, which is close to the pellet sintering temperature used in lab-scale FFC experiments. (Riekkola-Vanhanen 1999 p. 12, p. 23)

3.4 Oxygen content of chromite

To get information on the sintered chromite pellets composition and oxygen content, FESEM-EDS and XRF analyses were made. The FESEM-EDS analyzer and XRF of University of Oulu Centre of Material Analysis were used. The FESEM was Zeiss ULTRA Plus FESEM. The XRF analysis was done with PANalytical Axios max 4kW XRF. A pellet was analyzed in FESEM-EDS. The pellet was sliced in half, the surface was polished, and the pellet was baked into an epoxy resin. Carbon coating was also added for electric conductivity before analysis. Carbon was not included in the EDS -analysis results.

The results shown in Figure 12 and Table 5 show that chromium and iron oxides are the main elements in sintered chromite pellets. The black area in Figure 12 is the carbon coating. The dark gray areas consist mostly of SiO_2, but the pellet mainly consists of lighter elements consisting mainly of iron and chromium oxides (see Figure 12, Table 5).
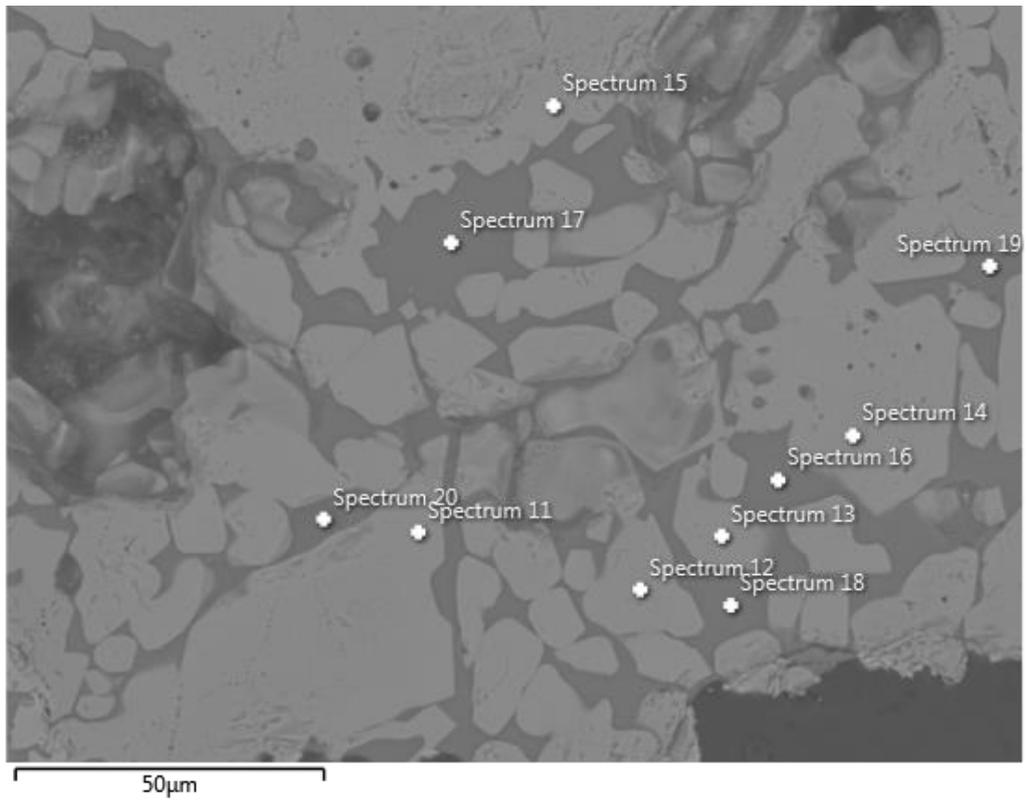
Figure 12. FESEM-EDS image of the pellet (EDS results in Table 5).

Table 5. EDS results for Figure 12.

Elements	Spectrum (wt-%)									
	11	12	13	14	15	16	17	18	19	20
O	35.61	35.45	35.28	38.33	35.28	48.07	44.18	44.24	43.96	44.76
Na							0.25			
Mg	6.12	6.48	6.35		4.84	2.51	1.58	2.85	2.02	1.21
Al	5.59	5.85	5.42		5.87	10.34	12.01	10.74	11.29	10.92
Si						26.49	27.77	28.53	29.41	28.99
K							0.21	0.22	0.13	0.25
Ca						4.75	6.99	4.63	5.54	6.87
Ti	0.22	0.26	0.34	0.2	0.21	1.2	1.26	1.13	1.17	1.43
V							0.28	0.23	0.18	0.32
Cr	36.67	36.41	36.63	37.12	35.75	0.78	0.55	0.78	0.75	1.26
Fe	14.92	15.54	15.98	16.06	18.05	5.87	4.91	6.66	5.14	3.58
Zn									0.41	0.41
Br				8.29						
Eu	0.88									
Tb				0						
Total	100	100	100	100	100	100	100	100	100	100

A very small area of pre-reduced iron was found in spectrum 35 and can be seen in Figure 13. It is also interesting to note that EDS detected some nickel and chromium in the iron (see Figure 13, Table 6).
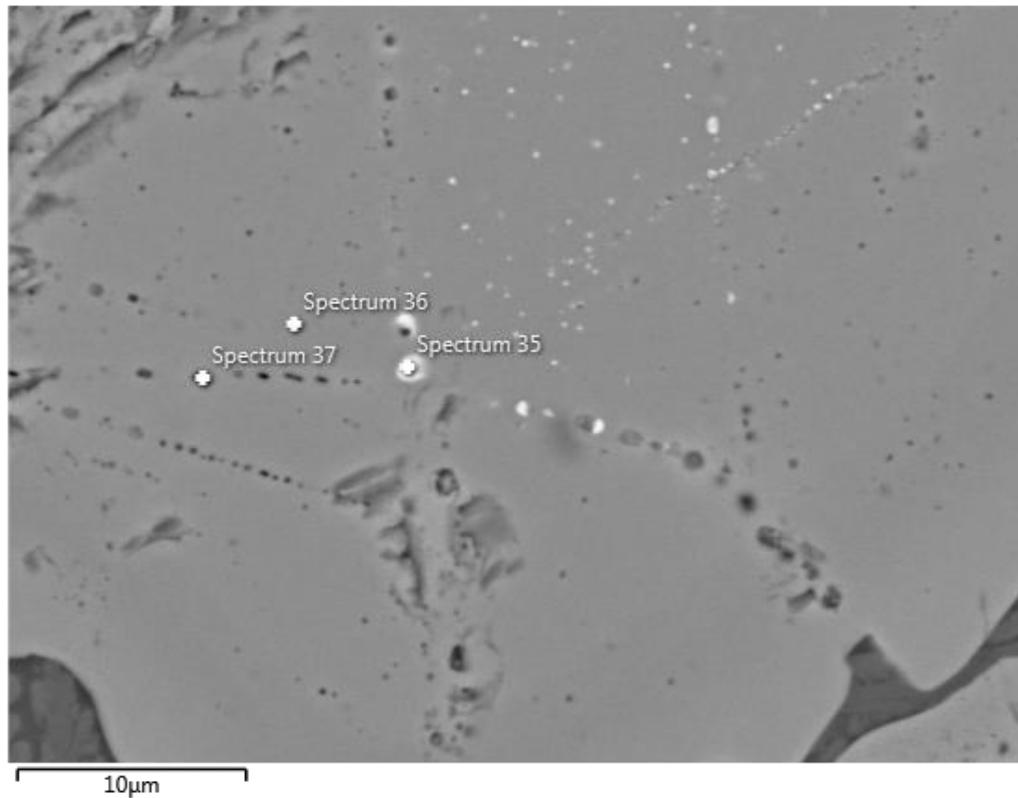
Figure 13. FESEM-EDS image of the pre-reduced iron (EDS results in Table 6).

Table 6. EDS results for Figure 13.

Elements	Spectrum (wt-%)		
	35	36	37
O		35.97	26.41
Mg		6.65	5.14
Al		8	7.26
Si			0.16
Ti		0.3	0.49
Cr	5.9	32.33	39.97
Fe	88.89	15.3	18.93
Ni	3.99		0.53
Ge		0.57	
Br	1.22		
Eu		0.88	1.12
Total	100	100	100

There was also a difference in the structure of the phases in the pellet halves. The other half contained streaks of heavier phases, and in the other half these streaks were absent. The chemical analysis of these two different pellets was still similar, with the heavier streaks containing less magnesium and slightly more iron (see Figure 14, Table 7).
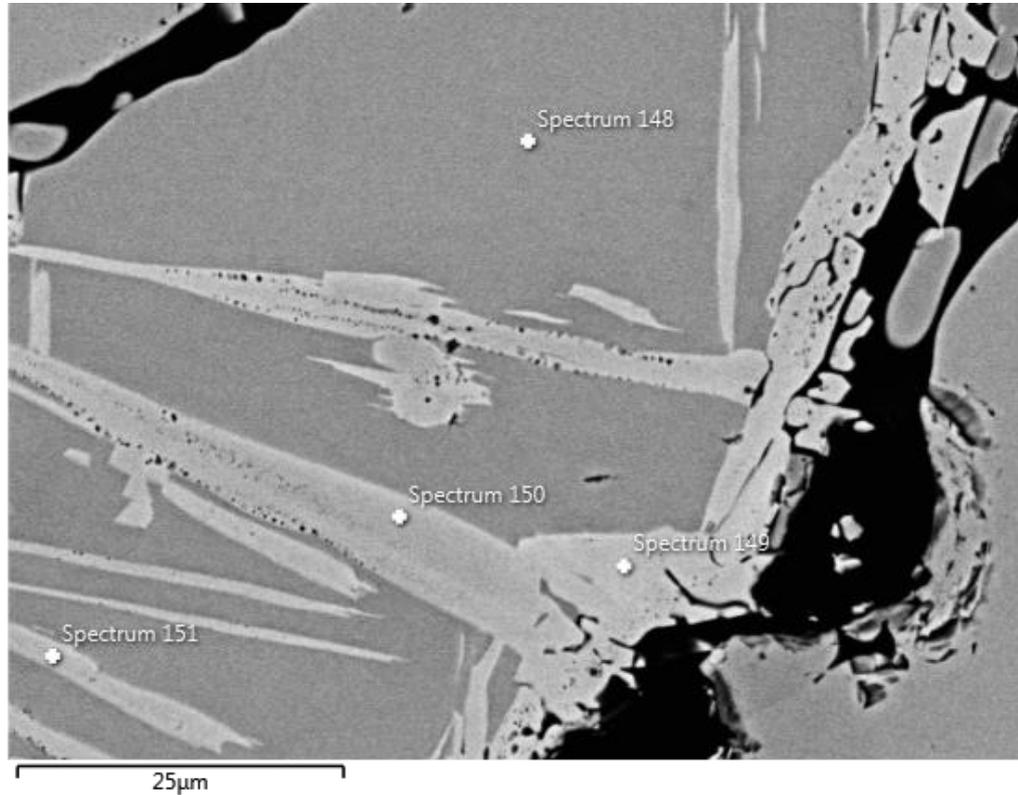
Figure 14. Streaky areas in the other half of the pellet (EDS results in Table 7).

Table 7. EDS results for Figure 14.

	Spectrum (wt-%)			
Elements	148	149	150	151
O	36.33	36.48	36.97	36.63
Mg	7.39			0.71
Al	6.82	8.03	9.24	7.72
Ti	0.26	0.62	0.93	1.22
Cr	31.54	33.26	34.57	36.81
Fe	16.49	21.61	18.28	16.91
Eu	0.91			
W	0.25			
Total	100	100	100	100

Overall structure of the pellets can be seen from Figure 15. The particle size seems to be much higher than the 5 micrometers recommended by Gordo et al. (2004).
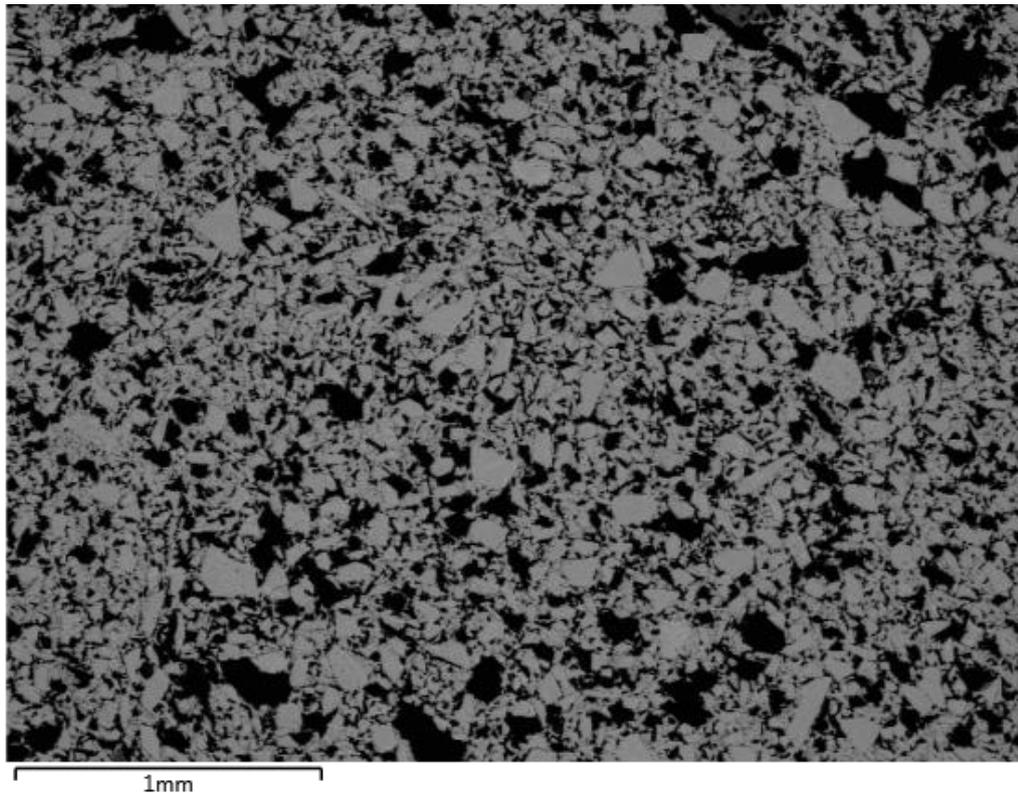
Figure 15. Image of a larger area of the pellet.

Five different areas were analyzed with the FESEM mapping feature and according to the EDS analysis, our pellet contained on average 36.97 wt-% O, 5.74 wt-% Mg, 6.79 wt-% Al, 2.73 wt-% Si, 0.34 wt-% Ti, 0.67 wt-% Ca, 0.004 wt-% K, 28.79 wt-% Cr, and 17.96 wt-% Fe.

Normalizing, and converting this to oxides we get 9.77 wt-% MgO, 43.18 wt-% Cr_2O_3, 26.35 wt-% Fe_2O_3, 6.00 wt-% SiO_2, 13.16 wt-% Al_2O_3, 0.96 wt-% CaO, 0.005 wt-% K_2O, and 0.58 wt-% TiO_2. For reference, a previous analysis by Heikkilä et al. (2015) shows that the pellets they used had 11 wt-% MgO, 44 wt-% Cr_2O_3, 19 wt-% Fe, 4 wt-% SiO_2, 13 wt-% Al_2O_3, and 0.5 wt-% CaO.

Figure 16 shows a compilation of the different mapped sections from both halves of the pellet. EDS analysis can be found in Table 8.
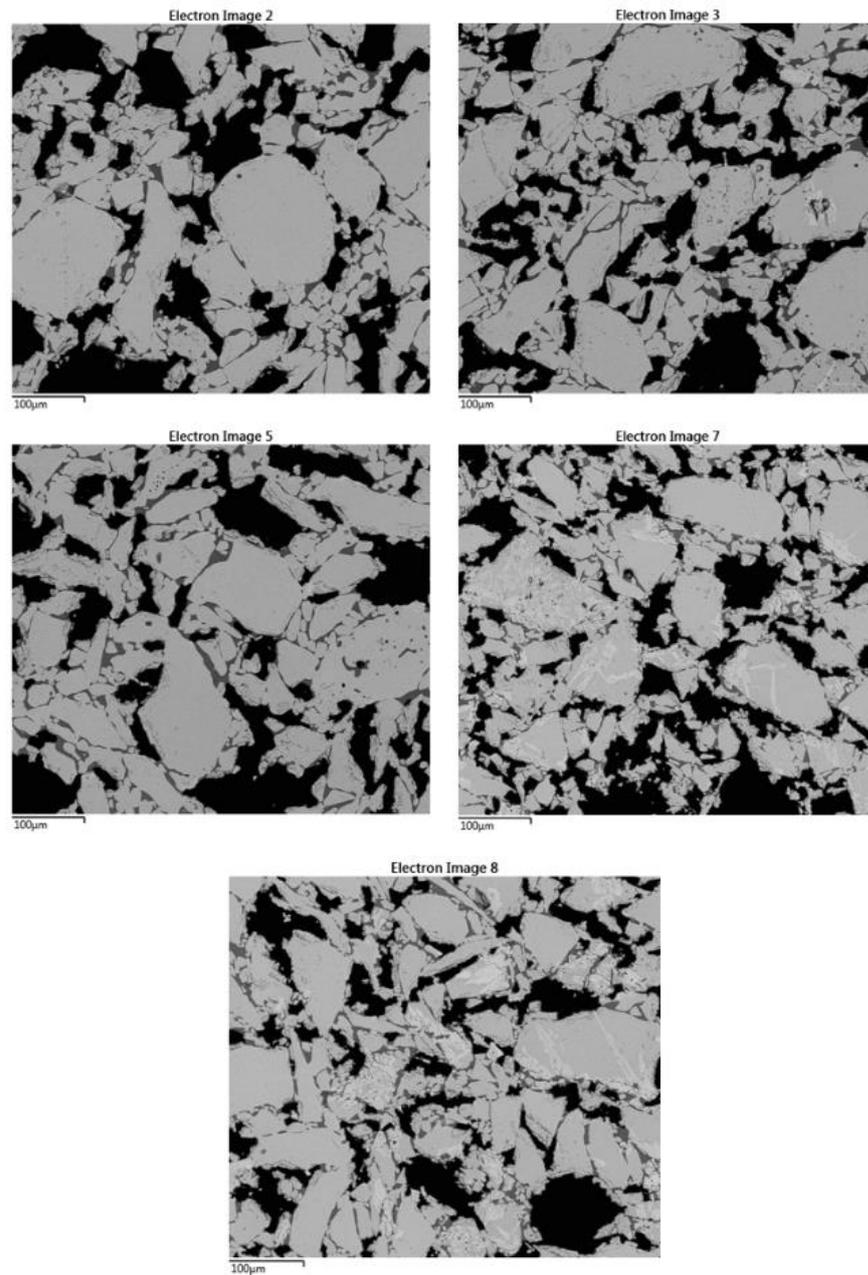
Figure 16. FESEM-EDS mapping areas used to measure the chemical composition of the pellet (EDS results in Table 8).

Table 8. EDS results for Figure 16.

Elements	Image (wt-%)				
	2	3	5	7	8
O	37.02	36.66	37.13	36.97	37.07
Mg	5.95	5.86	5.79	5.73	5.37
Al	6.66	6.9	6.78	6.75	6.85
Si	2.51	2.6	2.76	2.72	3.07
Ca	0.52	0.6	0.62	0.75	0.85
Ti	0.32	0.33	0.36	0.32	0.37
Cr	29.23	28.94	28.6	28.93	28.27
Fe	17.79	18.09	17.96	17.83	18.14
K	0	0.02	0	0	0
Total	100	100	100	100	100

XRF was also used to determine the amount of oxygen and composition of chromite. Fused bead analysis method was used. 10 analyses were made, with the fused beads containing 0.2 g of chromite. The oxide composition determined by XRF can be seen from Table 9.

Table 9. XRF analysis of chromite with the fused bead samples.

Fused bead XRF-samples	Sum before normalization	Sum	MgO	Al$_2$O$_3$	SiO$_2$	CaO	TiO$_2$	V$_2$O$_5$	Cr$_2$O$_3$	MnO	Fe$_2$O$_3$
	(wt-%)	(wt-%)	(wt-%)	(wt-%)	(wt-%)	(wt-%)	(wt-%)	(wt-%)	(wt-%)	(wt-%)	(wt-%)
1. Fused bead	105.003	100	10.752	13.052	4.047	0.653	0.595	0.199	43.000	0.280	27.422
2. Fused bead	100.280	100	10.786	12.810	4.009	0.645	0.535	0.230	43.299	0.312	27.373
3. Fused bead	100.133	100	10.886	13.491	3.953	0.732	0.599	0.194	42.540	0.258	27.347
4. Fused bead	106.726	100	10.910	13.238	4.091	0.629	0.546	0.124	42.841	0.320	27.299
5. Fused bead	106.909	100	11.044	13.030	4.090	0.687	0.519	0.224	42.798	0.273	27.335
6. Fused bead	104.536	100	10.964	13.070	4.060	0.644	0.553	0.165	42.726	0.278	27.539
7. Fused bead	97.013	100	10.790	12.859	4.117	0.634	0.507	0.211	43.100	0.288	27.493
8. Fused bead	101.780	100	10.747	12.738	4.089	0.726	0.513	0.168	43.130	0.382	27.507
9. Fused bead	104.073	100	10.838	13.142	4.031	0.705	0.575	0.188	42.759	0.324	27.437
10. Fused bead	109.207	100	10.978	13.037	4.158	0.717	0.499	0.197	43.144	0.331	26.939
Average	103.566	99.999	10.870	13.047	4.065	0.677	0.544	0.190	42.934	0.305	27.369
Normalized average		100	10.870	13.047	4.065	0.677	0.544	0.190	42.934	0.305	27.369

3.5 Experimental apparatus

The experimental apparatus used consisted of the custom furnace and gas flow assemblies. A power source connected to a laptop was used to provide the required voltages and record the experimental data. The anode, cathode assembly and molten salt crucible formed the electrolytic cell. The simplified schematic of the experimental apparatus can be seen in Figure 17. From Figure 18, we can see the furnace space where the crucible together with the pellet assembly was placed, and Figure 19 shows the graphite anode, crucible and gas flow assemblies.
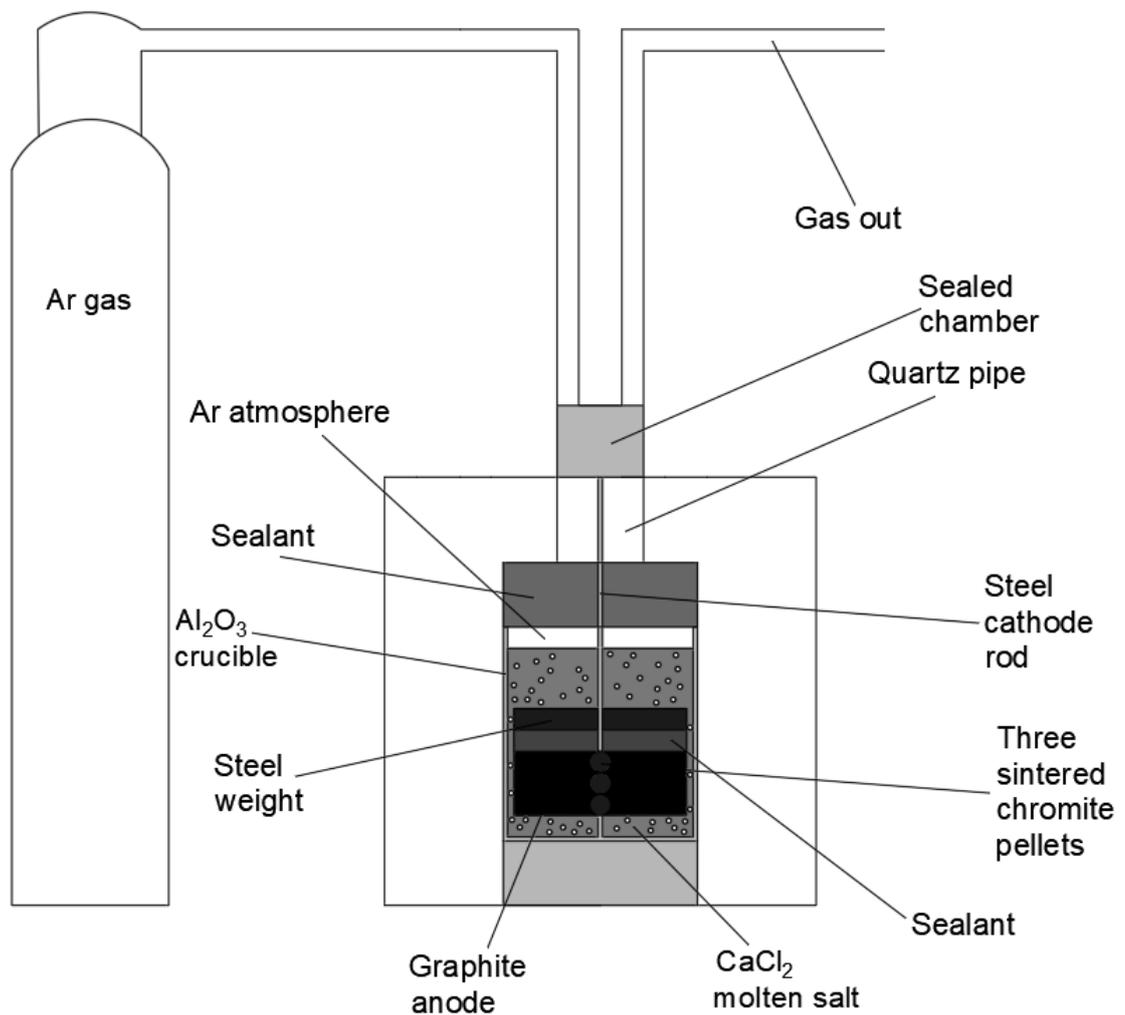

Figure 17. Simplified schematic of the FFC Cambridge process for manufacturing ferrochrome from sintered chromite pellets supplied by Outokumpu.
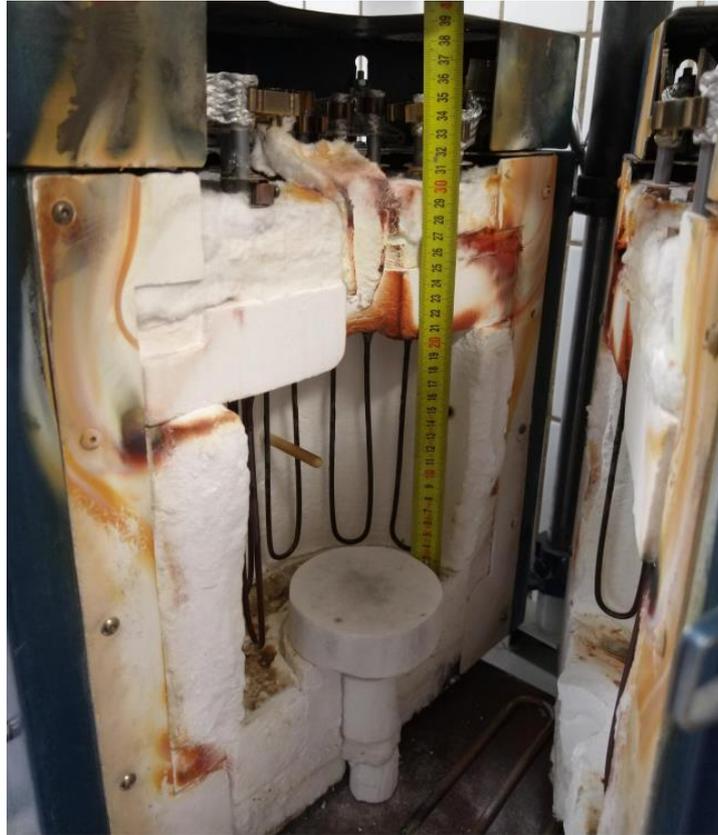
Figure 18. The FFC Cambridge furnace at the Process Metallurgy Research Unit.

Figure 19. Graphite anode, crucible and gas flow assemblies.

As for dimensions, the custom furnace has an octagonal cover with a 450 mm diameter, and the reactor space itself is cylindrical with a 200 mm diameter, covered by insulating material. The Al_2O_3 crucible is cylindrical with a 100 mm height, and a 90 mm diameter, the $CaCl_2$ powder was melted inside the crucible (see Figure 20). The carbon anode is ring-like with 80 mm diameter, 30mm height, 20 mm thickness, and a 40 mm diameter space at the middle is left for the pellet assembly (see Figure 20). The anode design was changed from a rod to a circle with the 40 mm diameter space in the middle for the electrolyte, since this provides more surface area for the anode, which is beneficial in lowering the voltage loss (Chen 2020). The anode starting weight was 216.10 g. The cathode was made of three sintered chromite ore pellets that were drilled from the middle to accommodate the 2-mm diameter steel connection rod, which can be seen in Figure 21. The power source was the BK precision 1696B power supply. Argon gas atmosphere was created by supplying the gas from a compressed gas cylinder. The heating of the reactor was powered by 10 heating resistors around the reactor.
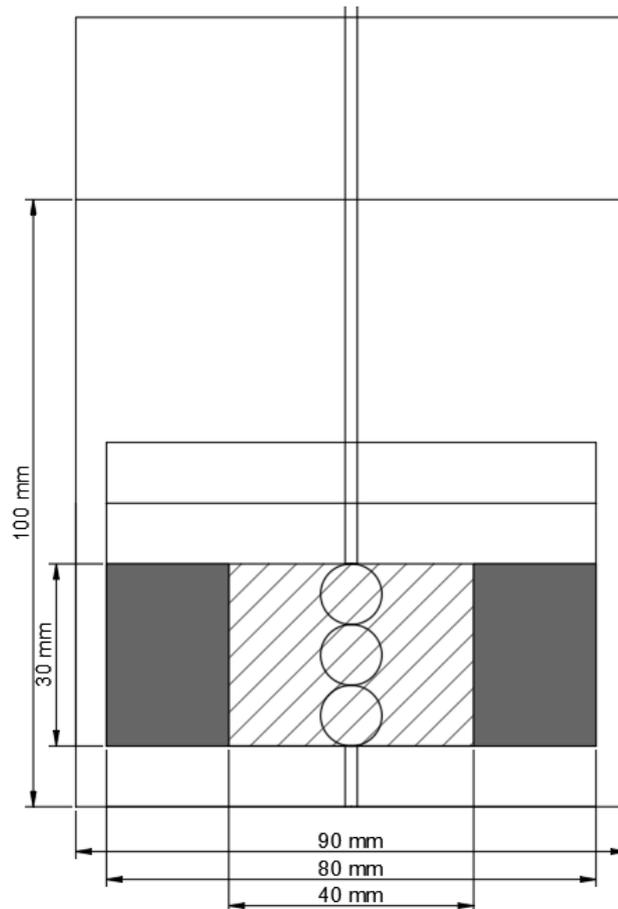

Figure 20. Dimensions of the crucible and the anode in millimetres.

The whole experimental setup had been planned to be air-tight to ensure that no oxygen or moisture could get inside the furnace. Different kinds of sealants were also used to ensure the sealed operation.

Figure 21. Pellet assembly.

3.6 Plan for the preliminary laboratory experiment

The first plan was to use parameters that have been previously considered adequate for chromite reduction to answer the first aim of this thesis: can chromite from the Kemi mine be reduced with a carbon anode. Ge et al. (2015) have studied chromite ore reduction and found that there was a reduction happening at 2.8 V and 900 °C. The sintering time the authors used was 3 hours and the temperature used was 1150 °C, which were deemed optimal, but in our first experiments, we will be using only chromite pellets that have been sintered at the Outokumpu Tornio works steel belt furnace at 1350 °C, since higher temperature sintered pellets have been adequately reduced in other studies (Gordo et al. 2004) as well. The particle size of our pellets is large in comparison with the other studies (see Figure 15). Gordo et al. (2004) have recommended under 5 micrometers as the maximum particle size. Since there was limited time to overview the different variables and their relationships, it was concluded that for the first test, best possible conditions

provided by the only available previous study on chromite reduction by Ge et al. (2015) were used.

The first test was done with a 1-hour electrolysis time at 2.8 V voltage and 900 °C temperature. Testing the effect of different electrolysis times was planned but was not conducted due to challenges that occurred during the experiments. Sintered pellets supplied and sintered by Outokumpu Tornio works were used as cathode pellets. The anode material was graphite. Alumina crucible was used as the reaction vessel. The molten salt used was $CaCl_2$. Ge et al. (2015) have recommended preheating the $CaCl_2$, chromite pellets, and the crucible in the oven at 110 °C to remove moisture (Ge et al. 2015). We used waterless $CaCl_2$ in our experiment, thus preheating was not needed as the possible water coming from the air should be decomposed from the $CaCl_2$ in the furnace during the preheating stage. The chromite preheating was done directly in the furnace, but the pellets were lowered gradually to the oven to prevent thermal shock and to remove the possible moisture from the pellets. Preheating the crucible was deemed unnecessary. The temperature was risen slowly at a rate of 2 °C/min until it reached 300 °C. The 300 °C temperature was kept for 1.5 hours, until it was risen to the designated 900 °C at a rate of 4 °C/min. The temperature of 900 °C was also planned to be sufficient for $CaCO_3$ decomposition (Gordo et al. 2004). The temperature of 900 °C should have been kept for 0.5-1.0 hours according to Ge et al. (2015), but we needed some extra time to fine-tune the temperature at the crucible to be 900 °C. The voltage was planned to be risen to 0.5 V for 0.5-1 hours, and after the voltage to be risen to 2.8 V, beginning the electrolysis at full voltage. The minimum voltage supplied by the power source was 1.0 V, thus it was selected instead of 0.5 V. Stepwise rising of the voltage is necessary for preventing overload of different reactions, since this can reduce the efficiency of electrolysis (Mohandas 2013).

After the electrolysis, the ferrochrome was cooled and washed with ethanol and dried. Washing with ethanol is necessary to prevent the reoxidation of ferrochrome to chromite (Mohandas 2013). Weighting was planned to be used in determining the reduction degree of the pellets, but this was unsuccessful, as the pellets were stuck on the cathode rod or disintegrated into the molten salt. The pellets went through FESEM-EDS analysis to look for possible areas with reduced ferrochrome. Carbon was not included in the EDS analysis.

The parameters that were monitored during the experiments were the voltage, time, current consumption, and anode weight change.

4 RESULTS AND DISCUSSION

4.1 Results from the first experiment

The experimental conditions for the first test were made with closely mimicking the parameters used by Ge et al. (2015). Argon gas flow was higher in our experiment to ensure inert operation and fulfilled the specified requirement for the cathode rod. The pre-electrolysis voltage minimum for our power source was 1.0 V, thus it was selected as the best alternative, even though lower may have been better to ensure reduction of iron oxides does not start immediately. In Table 10, these conditions are shown.

Table 10. Experimental conditions for the first FFC Cambridge experiment.

Experimental conditions	
Temperature (°C)	900
Pre-electrolysis time (h)	0.67
Pre-electrolysis voltage (V)	1.0
Electrolysis time (h)	1.0
Electrolysis voltage (V)	2.8
Molten salt	Waterless $CaCl_2$
Argon flow (L/min)	4 L/min
Anode material	Graphite

The experimental procedure started with adding 173.45 g of $CaCl_2$ into the crucible, which was enough to fill the whole crucible space with the graphite anode assembly. Next, programmed heating of the FFC Cambridge furnace was commenced. The first step aimed to achieve the pre-heating temperature of 300 °C at a rate of 2 °C/min, but the realized pre-heating temperature measured from the crucible was only approximately 285 °C. The pre-heating temperature was kept for 1.5 hours. The next heating step was done at a rate of 4 °C/min until an operation temperature of 900 °C was reached, which accounted for about 883 °C at the crucible (see Figure 22). This temperature was kept for

about 30 minutes. A slight adjustment was needed during the final heating to get the crucible temperature to 900 °C, after which the cathode wire together with the pellets was gradually lowered near the crucible to prevent thermal shock to the pellets.
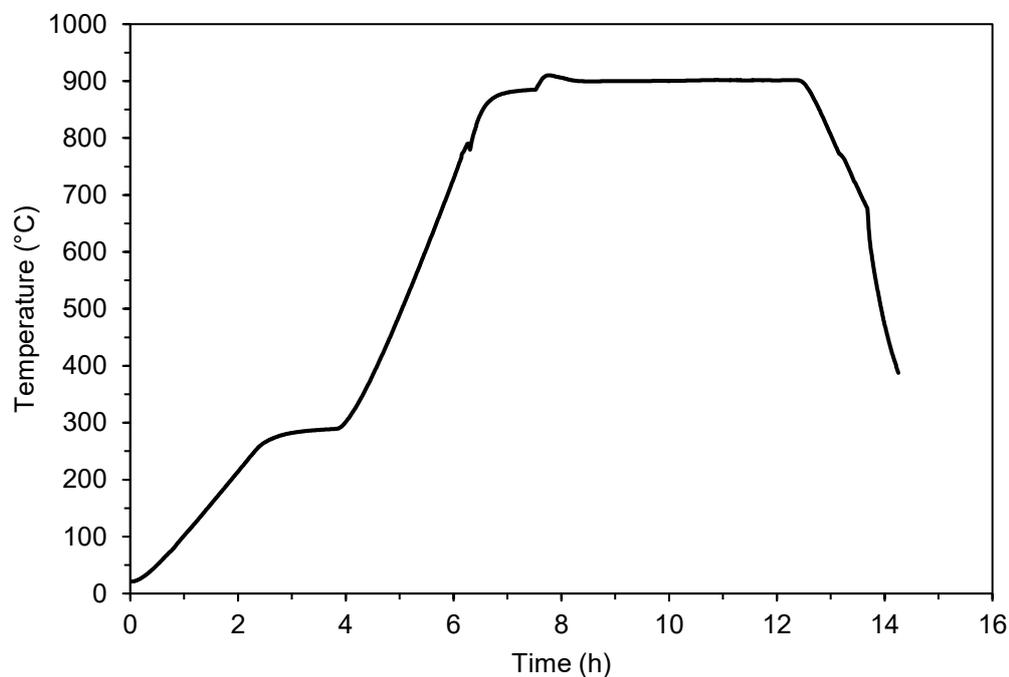

Figure 22. Temperature versus time graph of the experiment.

After the pellets were inserted into the crucible center and the molten salt, the potentiometer was connected to the ends of the contacts for the graphite anode and the steel cathode wire. The pre-electrolysis voltage was 1.0 V and time 40 minutes. Voltage was then increased with steps of 0.1 V until the operating voltage of 2.8 V was reached. During the experiment, the furnace built up pressure which lifted the top of the furnace assembly, which may have lifted the pellets out of the molten salt for a short while. The buildup of pressure was caused by the gas outlet clogging by a white substance, possibly evaporated $CaCl_2$. This was fixed during the experiment by opening a larger gas exhaust at the top of the furnace. The electrolysis at operating voltage lasted for about 1 hour, after which the cathode was pulled out from the molten salt into argon cooling. Two of the pellets dropped during this procedure, the highest pellet was left on the cathode. The pellet that was left was washed in a bucket of ethanol and left to dry in a laboratory oven at 105 °C over the weekend.

Figure 23 shows the current versus time and voltage versus time -plots of the experiment. In previous studies (Ge et al. 2015), the current versus time plots have an initial peak that

decreases in steps as the reduction progresses. Ge et al. (2015) suggested that the peak corresponds to the reduction of iron, followed by decreasing current as Cr_2O_3 is reduced (Ge et al. 2015). An example of Cr_2O_3-Fe_2O_3 reduction current versus time plot by Ge et al. (2015) is shown in Figure 24. The current versus time plot in our experiment showed clear peaks, but the downward stepwise graph that has been reported in other studies is absent. This may be due to inadequate contact with the molten salt, lifting or bending of the cathode rod during the experiment, or the pellets dropping.

At the end of the pre-electrolysis there was a current peak which started to settle, but it was followed by irregular current peaking during the stepwise increasing of the voltage, which then settled to about 0.7 A when voltage reached the target value of 2.8 V. At the recorded time of 1.66 h, there is also some irregular current behavior, which settled back to the 0.8 A -mark for the rest of the electrolysis. (see Figure 23)
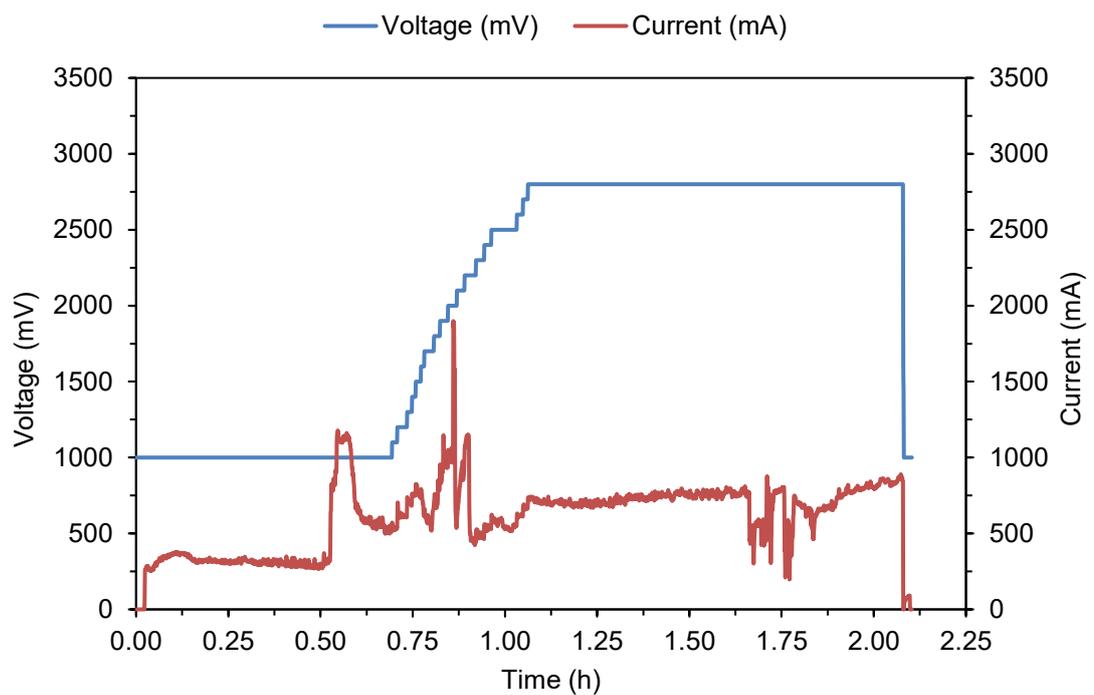

Figure 23. Current versus time and voltage versus time plot of the first experiment.
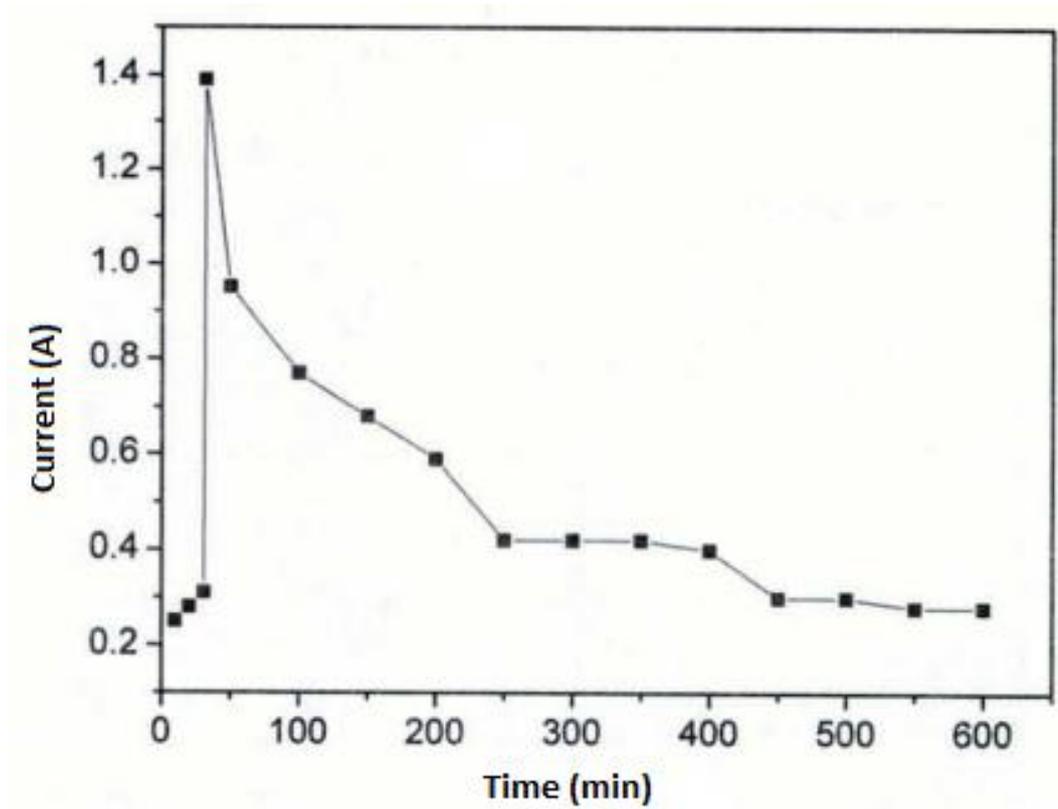
Figure 24. Current versus time plot from the study by Ge et al. (2015) (modified from Ge et al. 2015).

The analysis of the pellet that remained on the cathode and the two pellets that had dropped to the side of the crucible was done one week after the experiments. The pellets were cut in half and baked into epoxy and coated with carbon for FESEM-EDS analysis. Water -use during the cutting may have affected the samples, since some $CaCl_2$ may have leached off the pellet. The weighting of the pellets could not be done, as the cathode wire was stuck in the pellet center, thus the analysis of reduction the degree was unsuccessful.

In Figure 25, the cathode rod and the only pellet left are visible. The last remaining pellet appears to be one to two pellet's distance away from the knot tied to the end of the cathode rod. Dropped pellets were recovered from the top of the crucible for analysis and can be seen in Figure 26. The pellets that dropped may have been dropped during the lifting of the cathode rod, as there was quartz tubing around the graphite anode hole. Figure 26 also shows that there is little $CaCl_2$ left in the crucible.

Figure 25. Pellet remaining on the cathode after electrolysis.

Figure 26. Pellets dropped on the crucible weight.

The cathode-pellet contact area FESEM image for the only pellet remaining on the cathode rod is visible in Figure 27. The space between the electrode and the pellet is filled with $CaCl_2$, which is indicated by the EDS results for spectrum 12 (see Figure 27, Table 11). No reduced ferrochrome was found, as only chromite and $CaCl_2$ was detected in EDS results for spectrums 6,7,9, and 11 (see Figure 27, Table 11).

Figure 27. Analysis of the cathode wire and pellet contact area of the chromite pellet remaining on the cathode rod (EDS results in Table 11).

Table 11. EDS results for Figure 27.

Elements	Spectrum (wt-%)					
	6	7	8	9	11	12
O	26.17	25.05		30.38	11.84	29.54
Mg	10.62	10.66		9.77	3.18	0.91
Al	8.23	8.2		8.32	10.79	1.26
Si			0.81			2.68
Cl	0.74	1.65		0.49	5.73	21.75
Ca	0.18	0.82		0.16	1.27	18.43
Ti		0.27			0.78	0.58
V						5.76
Cr	36.68	38.31	20.63	35.22	45.61	12.36
Mn			2.08			
Fe	17.4	15.03	66.78	15.68	20.8	6.72
Ni			9.7			
Total	100	100	100	100	100	100

Analysis of a larger areas of the pellet remaining on the cathode rod displayed in Figure 28 also indicated the presence of chromite with some calcium chloride (see Figure 28, Table 12).
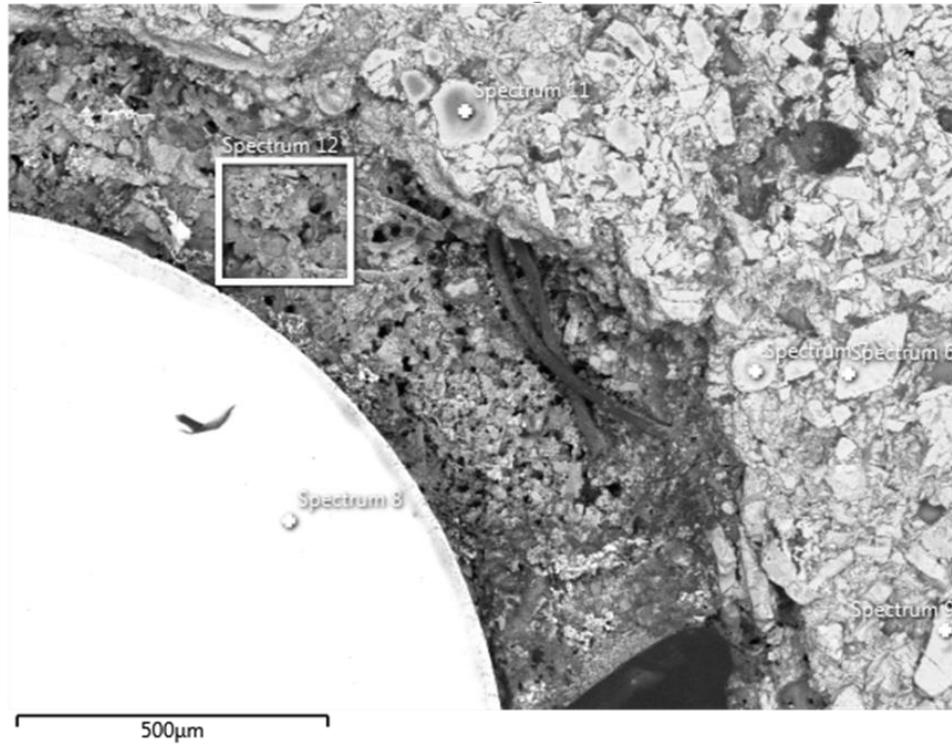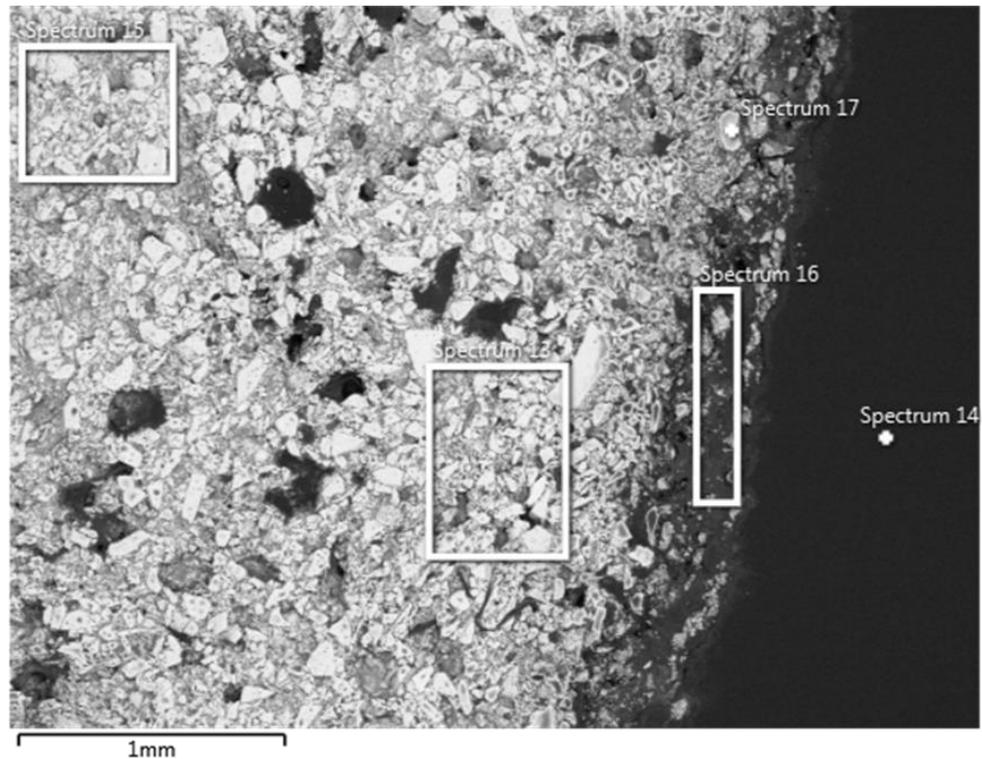
Figure 28. Analysis of the edge of the chromite pellet remaining on the cathode rod (EDS results in Table 12).

Table 12. EDS results for Figure 28.

Elements	Spectrum (wt-%)				
	13	14	15	16	17
O	30.14	71.94	31.97	38.95	25.35
Mg	5.7		5.6	3.78	6.89
Al	6.82		6.37	4.37	9.18
Si	2.39		2.51	1.78	
Cl	2.96	28.06	4.73	16.67	1.29
Ca	3.29		4.42	6.96	0.16
Ti	0.3				
Cr	30.19		27.63	19.19	36.77
Fe	18.2		16.77	8.31	20.37
Total	100	100	100	100	100

FESEM-EDS revealed that the two dropped pellets had some iron left in them, however many of the EDS -analysis spots contained nickel, which may indicate the presence of cathode rod pieces (see Table 13). Spectrum 73 shows the $CaCl_2$, which was also abundant in the samples (see Figure 30, Table 15). Analysis of the nickel -containing

metal is shown in Figure 29 and the EDS results are displayed in Table 14. A larger magnification of the metal with the EDS analysis are displayed in Figure 30 and Table 15.

Table 13. The elemental composition of the cathode rod.

Elements (wt-%)						
C	Si	Mn	Cr	Ni	N	Fe
0.07	1.60	0.60	21.00	10.00	0.15	66.58
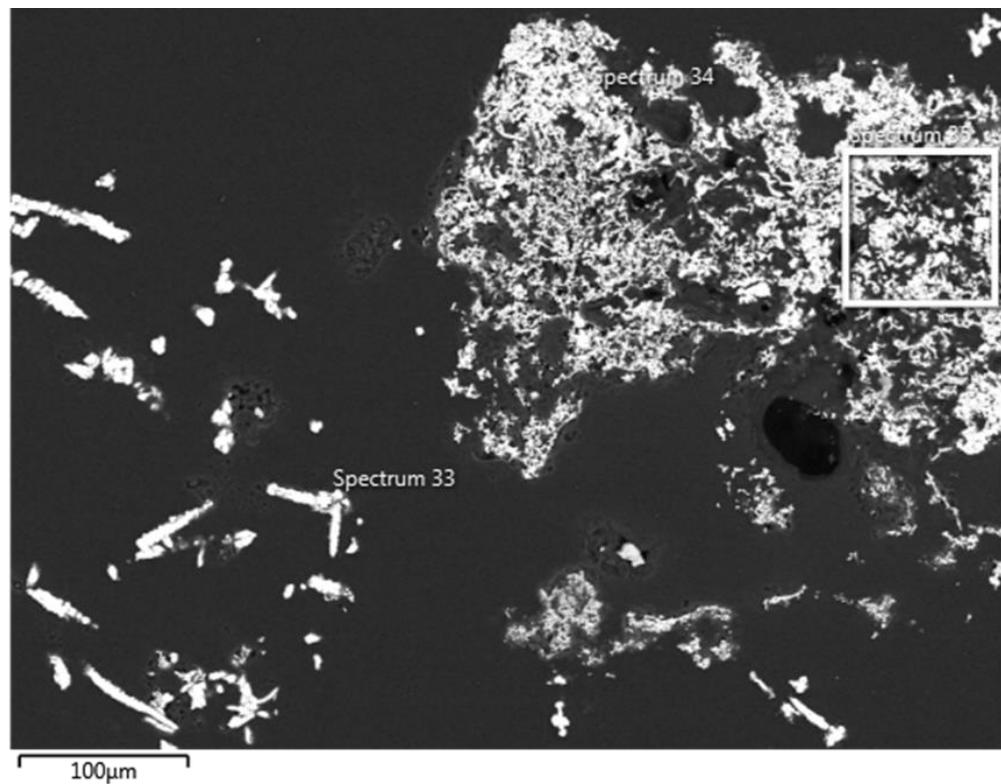
Figure 29. Metal particles in the dropped samples (EDS results in Table 14).

Table 14. EDS results for Figure 29.

Elements	Spectrum (wt-%)		
	33	34	35
O		3.42	6.65
F		1.62	
Al			0.74
Si	0.88	2.57	2.1
P	0.28	0.28	0.44
S			0.19
Cl	0.13	0.7	4.03
Ca	0.27	2.87	1.51
Ti		0.55	0.46
V	0.26	0.45	0.57
Cr	0.71	0.7	0.68
Fe	93	83.7	80.82
Ni	4.08	2.53	1.81
Br		0.61	
Mo	0.4		
Total	100	100	100
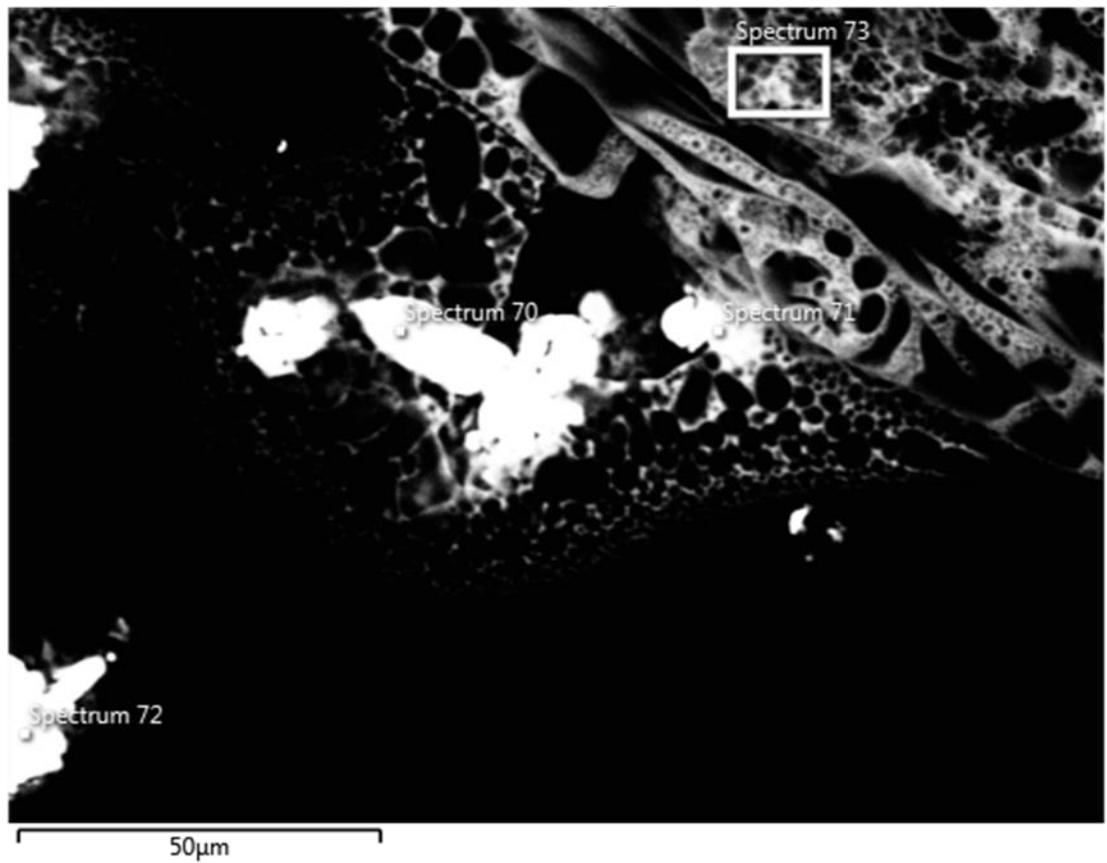
Figure 30. analysis of metal particle (EDS results in Table 15).

Table 15. EDS results for Figure 30.

Elements	Spectrum (wt-%)			
	70	71	72	73
O	1.38	0.49		21.7
Si	0.22	0.68	0.25	
P	0.5	0.4	0.35	
Cl	1.56	5.13	0.23	48.22
K				0.19
Ca	1.24	3.07	0.42	28.33
Ti		0.22		
V	0.57	0.91		
Cr	0.42	1.08	0.25	
Fe	92.49	84.5	93.72	1.55
Ni	1.63	3.29	4.77	
Br		0.22		
Total	100	100	100	100

It can be seen from the EDS analysis for Figure 31's spectrum 43 that no oxygen or nickel -containing iron was formed on the other dropped pellet surrounded by molten salt. The EDS analysis is displayed in Table 16. This may have been the lowest pellet due to better contact with the molten salt, thus achieving better reduction.
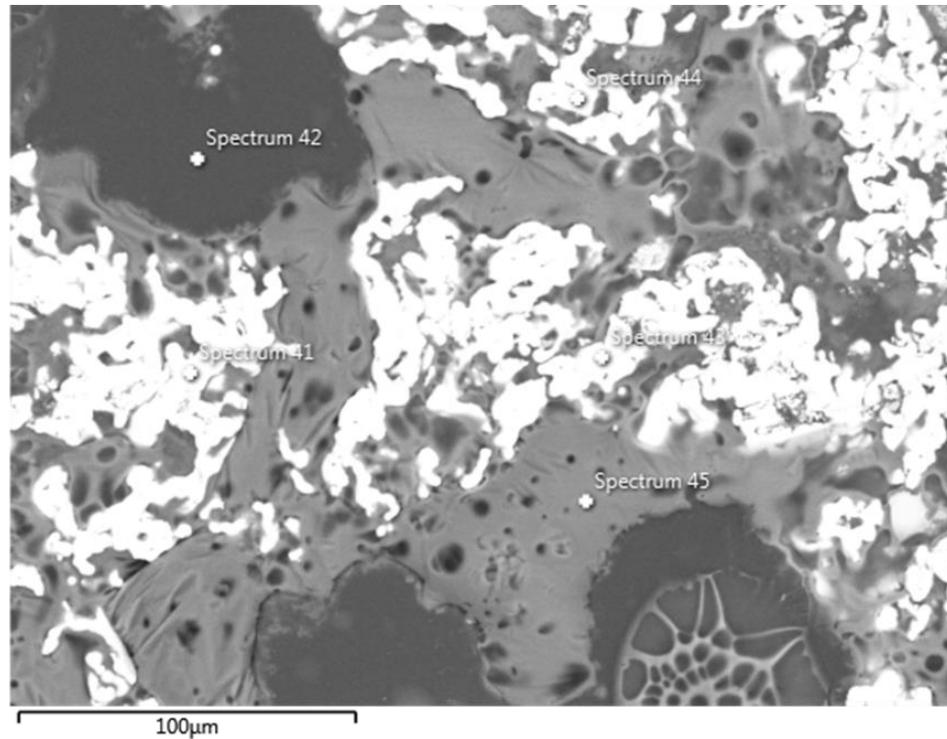
Figure 31. Metal on the dropped pellet samples (EDS results in Table 16).

Table 16. EDS results for Figure 31.

| Elements | Spectrum (wt-%) | | | | |
	41	42	43	44	45
O	3.07	38.61			9.92
Mg	0.87				
Al	2.16				
Si					0.25
P	0.42		0.44	0.6	
Cl	0.21	52.66	0.27		22.18
Ca	0.28		0.31	0.14	15.12
Ti	0.29				
Cr	0.4				
Fe	91.2	8.73	98.97	98.24	52.52
Ni	1.1			1.02	
Total	100	100	100	100	100

Figure 32 shows a smaller magnification of the sample. The sample contained large areas of $CaCl_2$, areas with the metal and the salt, and areas where there was only metal.
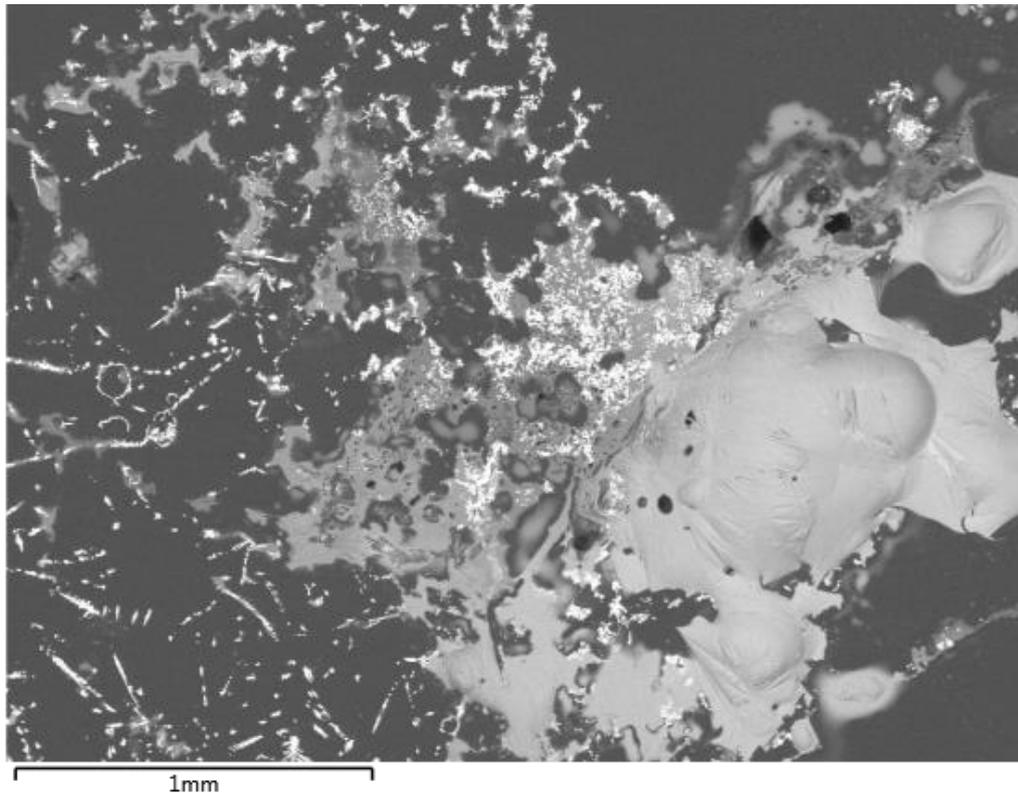
Figure 32. Metal and $CaCl_2$ on the dropped pellet samples.

The anode bound to the crucible by molten salt was left in water to be analyzed. Pieces of chromite pellets were found from the solidified molten salt. Same procedure for sample manufacturing was employed as with the pellet pieces recovered after the experiments. Also, three solid samples from the suspension were analyzed with FESEM-EDS. Analysis of the pellet pieces found in the molten salt show that small areas were reduced. One piece of the pellet did not contain any reduced ferrochrome, which can be seen in Figure 33.

Figure 33. FESEM image of the unreduced piece of chromite.

However, in the other found piece, there was a very small area of individual reduced chromite particles at the edge of the pellet. These can be seen in Figure 34.
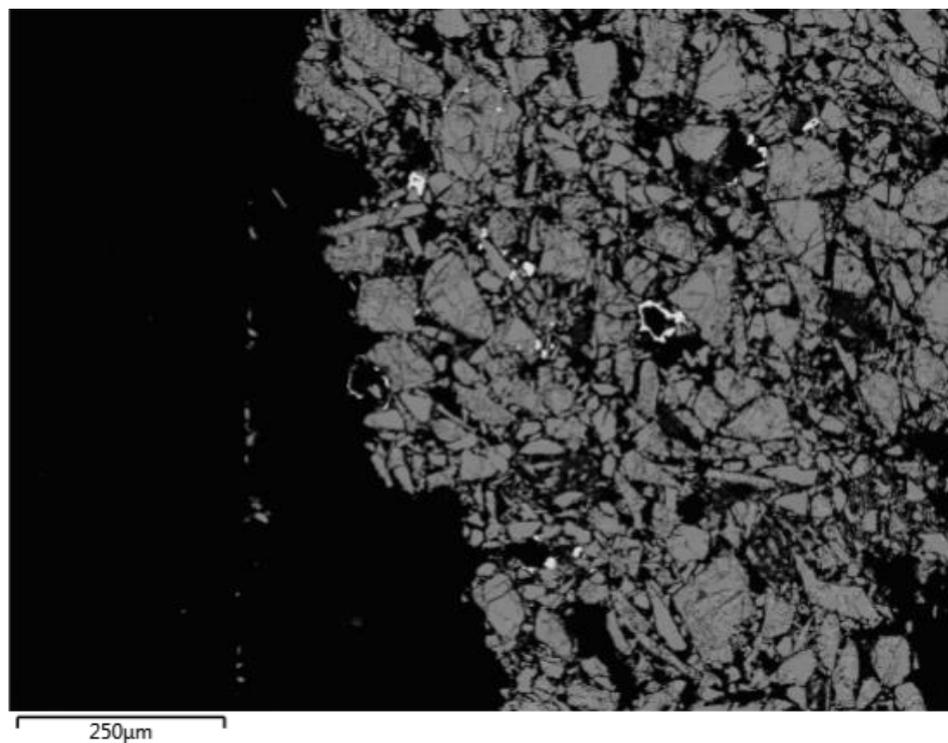
Figure 34. small area of reduced chromite.

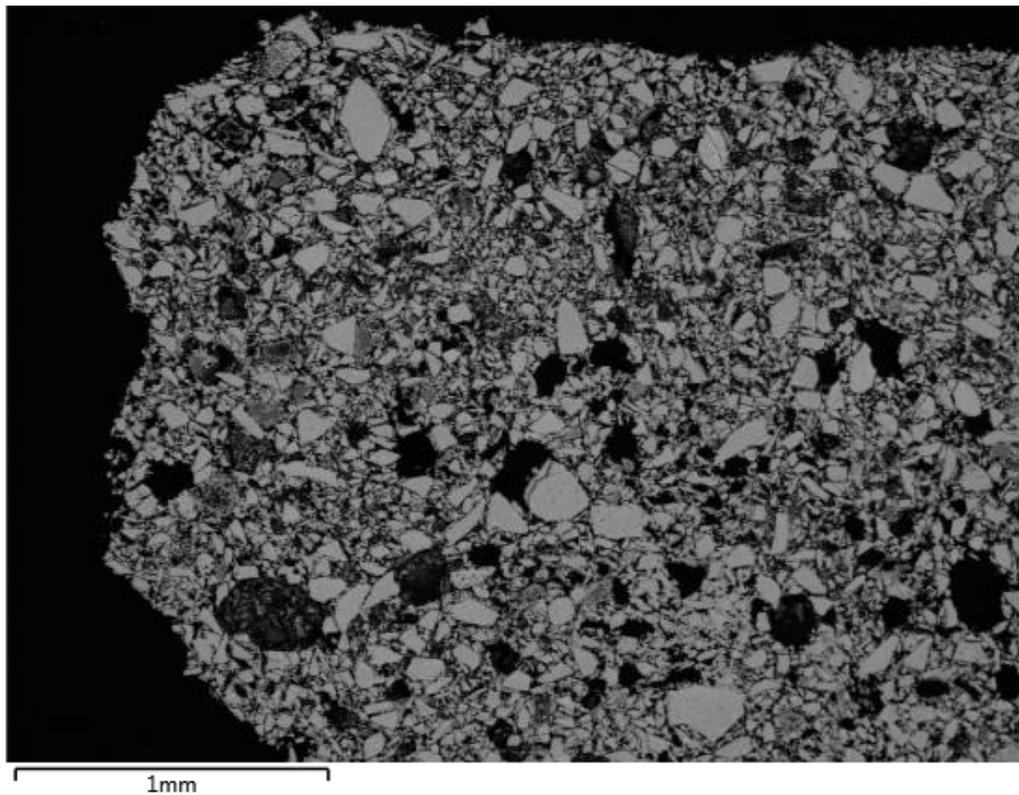Figure 35 and Table 17 show a larger magnification of an individual reduced particle of chromite with the EDS analysis. The ferrochrome contains very little chromium, only a little over 2 wt-%, as indicated by spectrums 114–116.
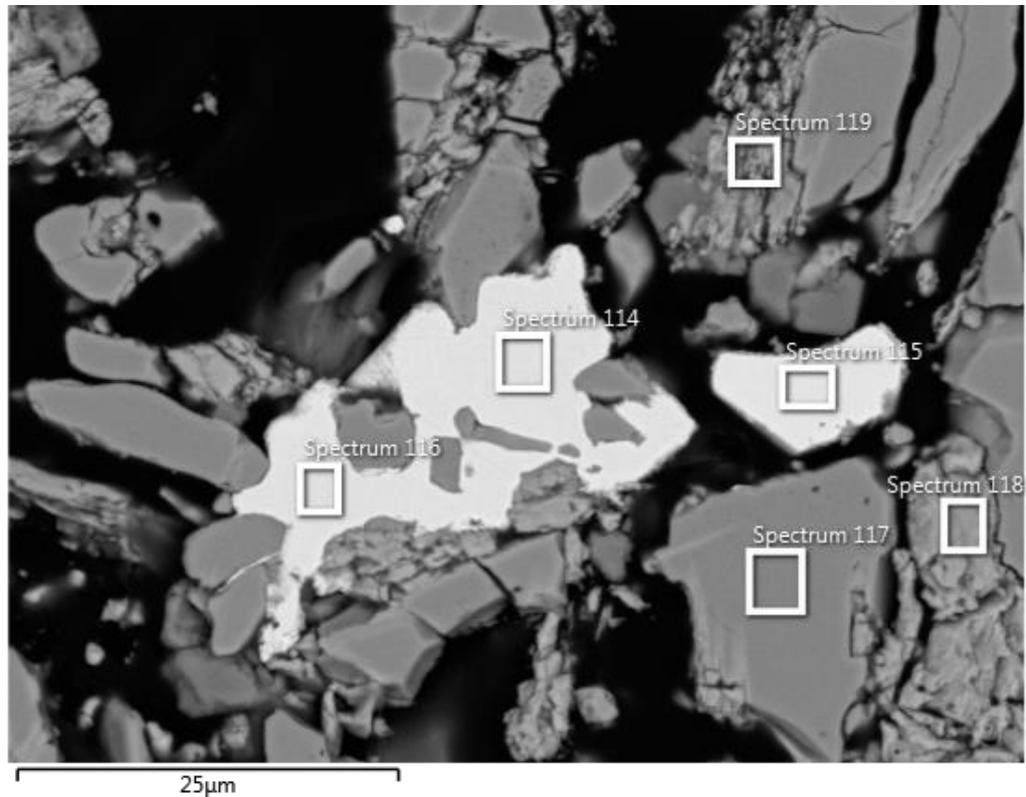
Figure 35. Reduction of individual particles of chromite (EDS results in Table 17).

Table 17. EDS results for Figure 35.

	Spectrum (wt-%)					
Elements	114	115	116	117	118	119
N						11.74
O				31.37	28.4	25.03
Mg				10.81	3.73	2.6
Al				7.02	8.07	7.88
Si					0.37	2.09
Cl						2.37
Ca					0.29	3.88
Ti				0.19	0.34	0.28
V					0.73	1.51
Cr	2.34	2.47	2.69	35.52	37.58	26.96
Fe	97.66	97.53	97.31	15.08	20.48	15.66
Total	100	100	100	100	100	100

Figure 36 shows similar analysis results for the reduced chromite as with Figure 35. The EDS results for Figure 36 are displayed in Table 18.
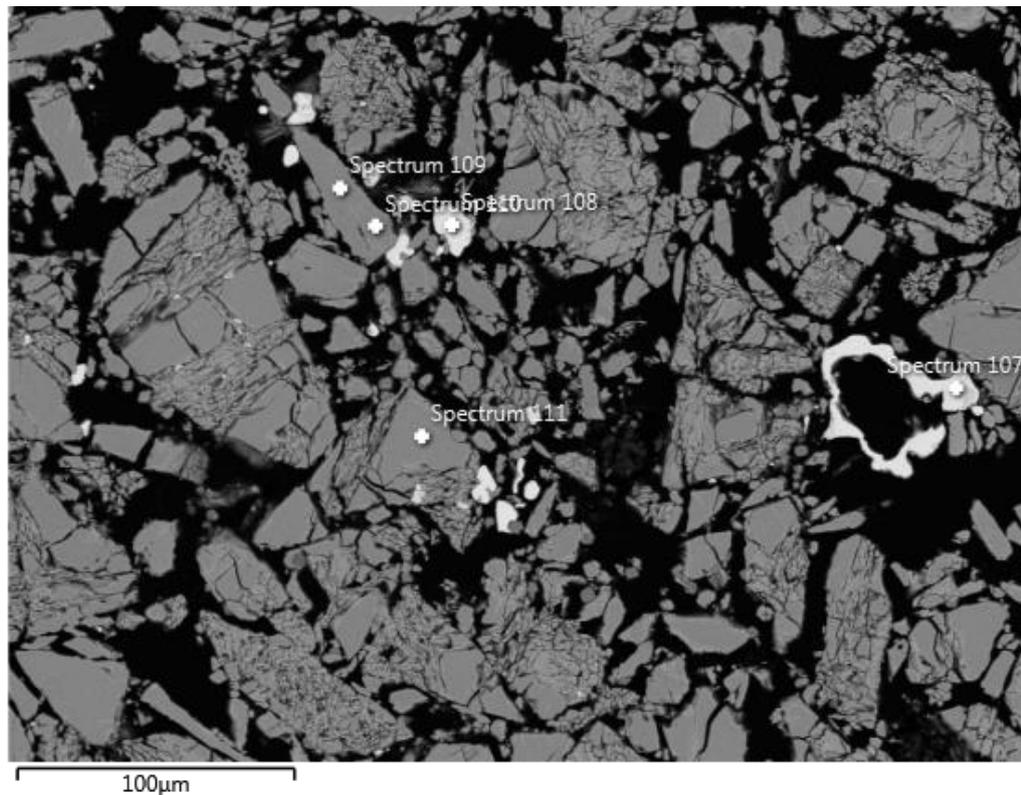
Figure 36. Ferrochrome found from the chromite samples at the bottom of the crucible (EDS results in Table 18).

Table 18. EDS results for Figure 36.

	Spectrum (wt-%)				
Elements	107	108	109	110	111
O			31.12	31.62	31.2
Mg			11.06	10.99	10.56
Al			6.97	7.19	7.01
Ti					0.24
Cr	3.08	2.33	35.89	35.37	35.34
Fe	96.92	97.67	14.96	14.82	15.65
Total	100	100	100	100	100

The suspension also contained reduced chromite. However, when looking at the FESEM imagery, the reduction process seems to negatively affect the mechanical integrity of individual chromite particles, as there seems to be an abundance of cracks visible in the FESEM images (see Figure 37). This may have resulted in the dropping of the pellets

from the cathode rod. The suspension samples contained the highest chromium content for ferrochrome at 7.87 wt-%. Also, 0.22 wt-% of vanadium was detected in the reduced area by EDS. This can be seen in Figure 37's spectrum 175 (see Table 19).
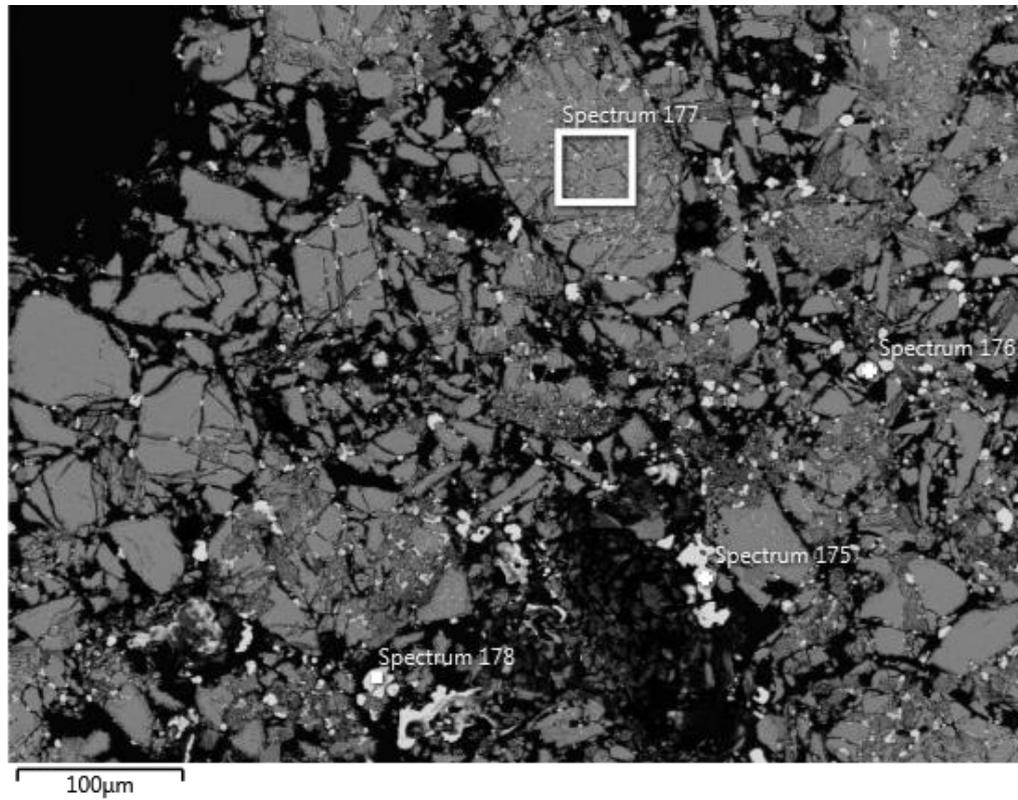
Figure 37. Reduced chromite in the suspension (EDS results in Table 19).

Table 19. EDS results for Figure 37.

	Spectrum (wt-%)			
Elements	175	176	177	178
O			27.4	
Mg			5.57	
Al			8.14	
Si			0.2	
Cl			0.52	
Ca			0.89	
V	0.22			
Cr	7.87	2.68	38.87	2.44
Fe	91.91	97.32	18.4	97.56
Total	100	100	100	100

In Figure 38, a large area of chromite has been partially reduced. The partially reduced area seems to have many cracks. The reduced particles contain only iron and chromium, which indicates the presence of ferrochrome (see Figure 38, Table 20). A larger magnification of the reduced ferrochrome particles of Figure 38 is displayed in Figure 39. The EDS results of Figure 39 are displayed in Table 21. The highest amount of chromium for these datapoints at 7.4 wt-% is found in spectrum 97 (see Figure 39, Table 21).
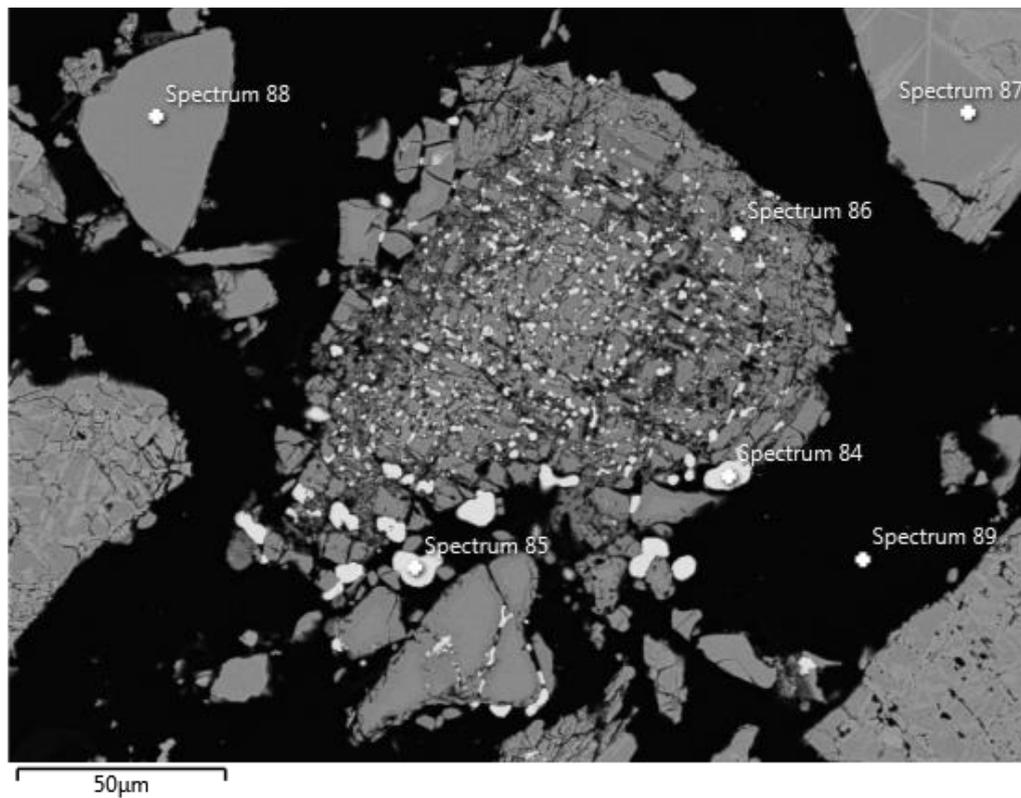
Figure 38. Brittling reduction of chromite (EDS results in Table 20).

Table 20. EDS results for Figure 38.

	Spectrum (wt-%)					
Elements	84	85	86	87	88	89
O				30.71	30.98	57.77
Mg				9.68	9.86	
Al				7.5	6.6	
Cl						35.18
Ti					0.27	
Cr	3.29	3.4	4.56	36.63	37.03	7.05
Fe	96.71	96.6	95.44	15.49	15.26	
Total	100	100	100	100	100	100
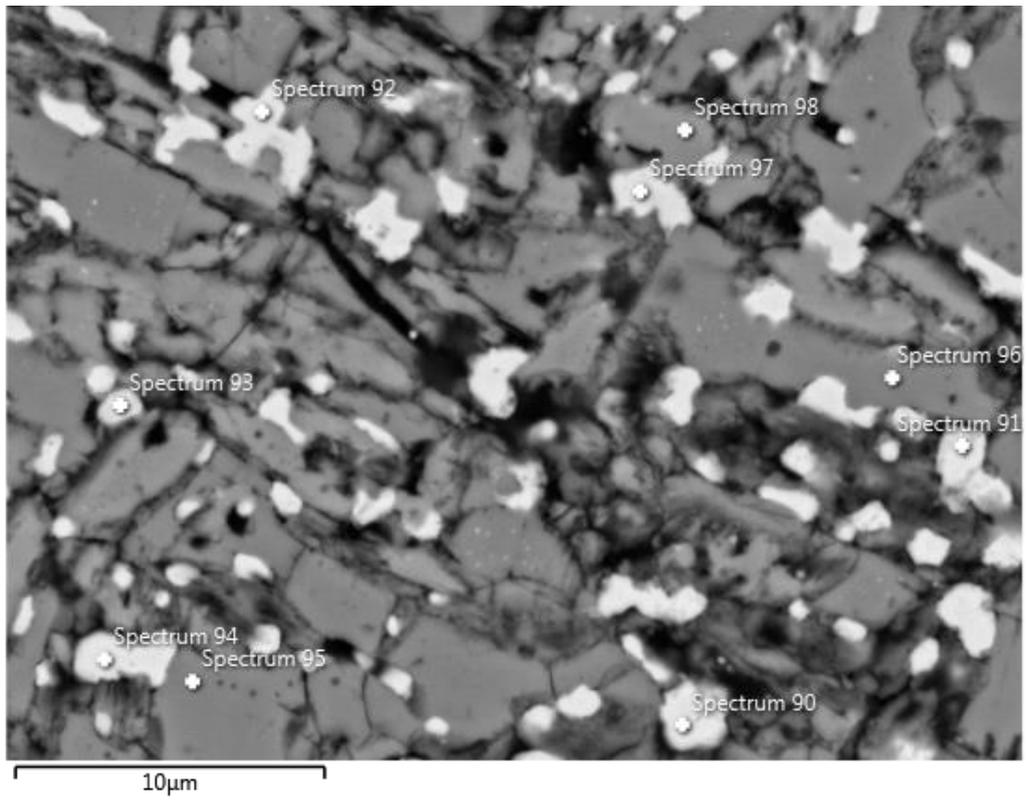
Figure 39. Larger magnification of the brittling chromite reduction (EDS results in Table 21).

Table 21. EDS results for Figure 39.

Elements	Spectrum (wt-%)								
	90	91	92	93	94	95	96	97	98
O						30.95	29.49		32.22
Mg						10.73	10.37		2.07
Al		0.37		0.3		9.21	9.54		12.64
Ca	0.17				0.13	0.2	0.42		0.21
Ti									0.88
V						0.41	0.45		
Cr	4.81	4.88	5.46	5.39	5.34	42.03	40.55	7.4	42.75
Fe	95.02	94.75	94.54	94.31	94.52	6.48	9.19	92.6	9.23
Total	100	100	100	100	100	100	100	100	100

Iron particles, which contained over 12 wt-% nickel were also abundant in the suspension samples. These show that the cathode wire did not withstand the electrolysis process. Figure 40 illustrates the large area of metal droplets found from the sample. Table 13 shows the composition for the cathode rod. The composition should contain 10 wt-% nickel, but analysis of some metal droplets from the solid samples gathered from the suspension contain even higher amounts of nickel, for example in Figure 41 spectrum 78, the EDS analysis indicates nickel content of 14.09 wt-%. The EDS results for Figure 41 are illustrated in Table 22.
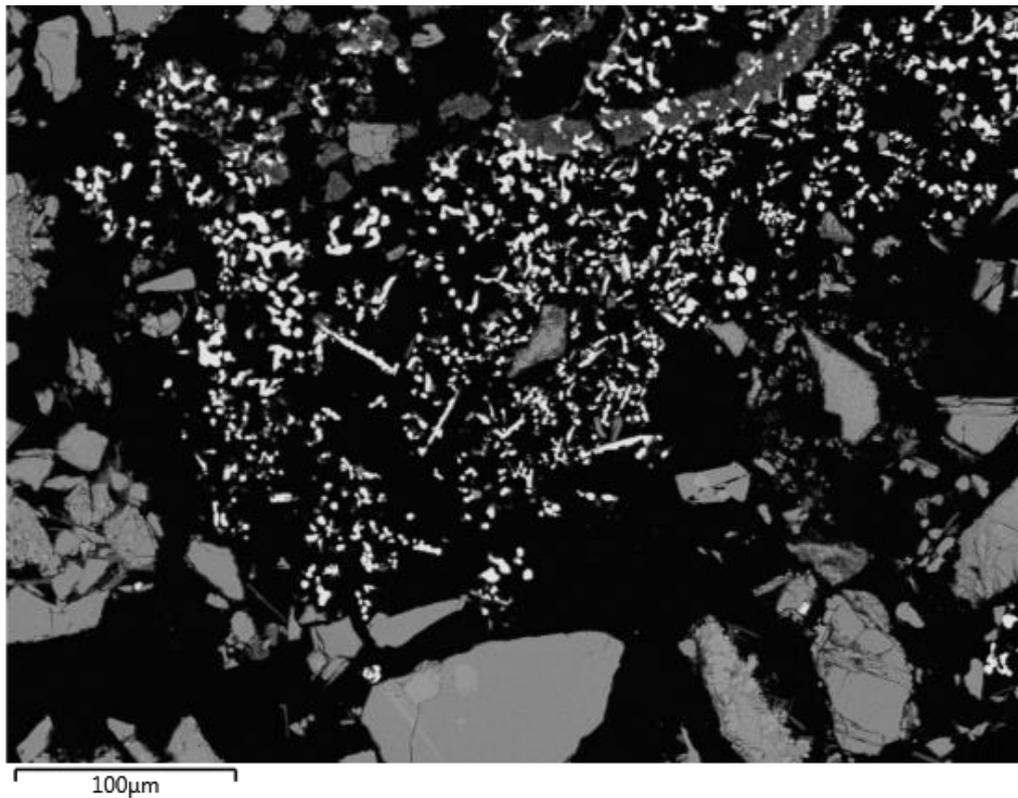
Figure 40. Lower magnification of the suspension sample.
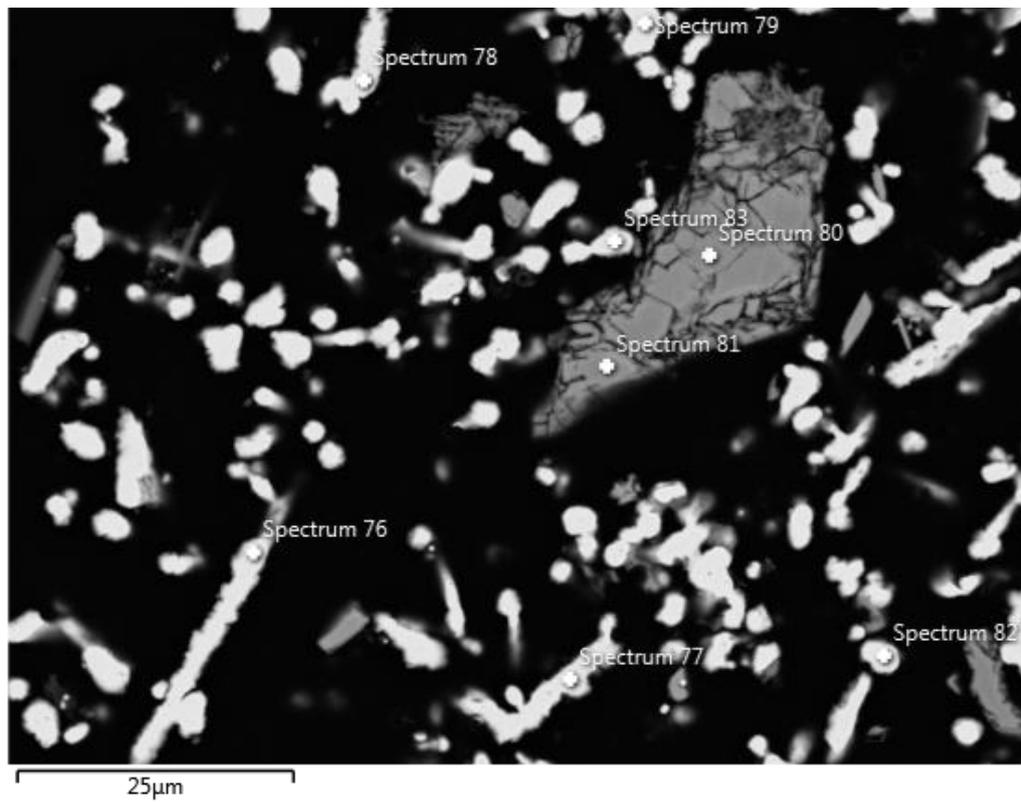
Figure 41. Nickel particles in the suspension sample (EDS results in Table 22).

Table 22. EDS results for Figure 41.

	Spectrum (wt-%)							
Elements	76	77	78	79	80	81	82	83
O					29.66	30.62		
Mg					7.95	8.09		
Al					8.13	7.75		
V			0.38	0.39	0.39		0.37	0.22
Cr	0.67	0.79	0.98	0.72	31.88	31	1.31	1.22
Fe	85.68	85.89	84.54	85.14	21.99	22.54	85.93	85.27
Ni	13.65	13.32	14.09	13.75			12.38	13.3
Total	100	100	100	100	100	100	100	100

Electrode degradation was clearly visible in analyses of areas with the cathode rod. Figures 42 and 43 show FESEM imagery from the cut pieces from the bottom knot of the cathode. Figure 42 shows a large area of cathode metal pieces, and the edge of the cathode seems to be corroded by the molten salt. Analysis of the metal pieces was made in Figure 43, and the chemical composition seems to go well with the reported values for the cathode rod (see Table 13). Table 23 shows the EDS results for the broken-off pieces of metal for Figure 43.
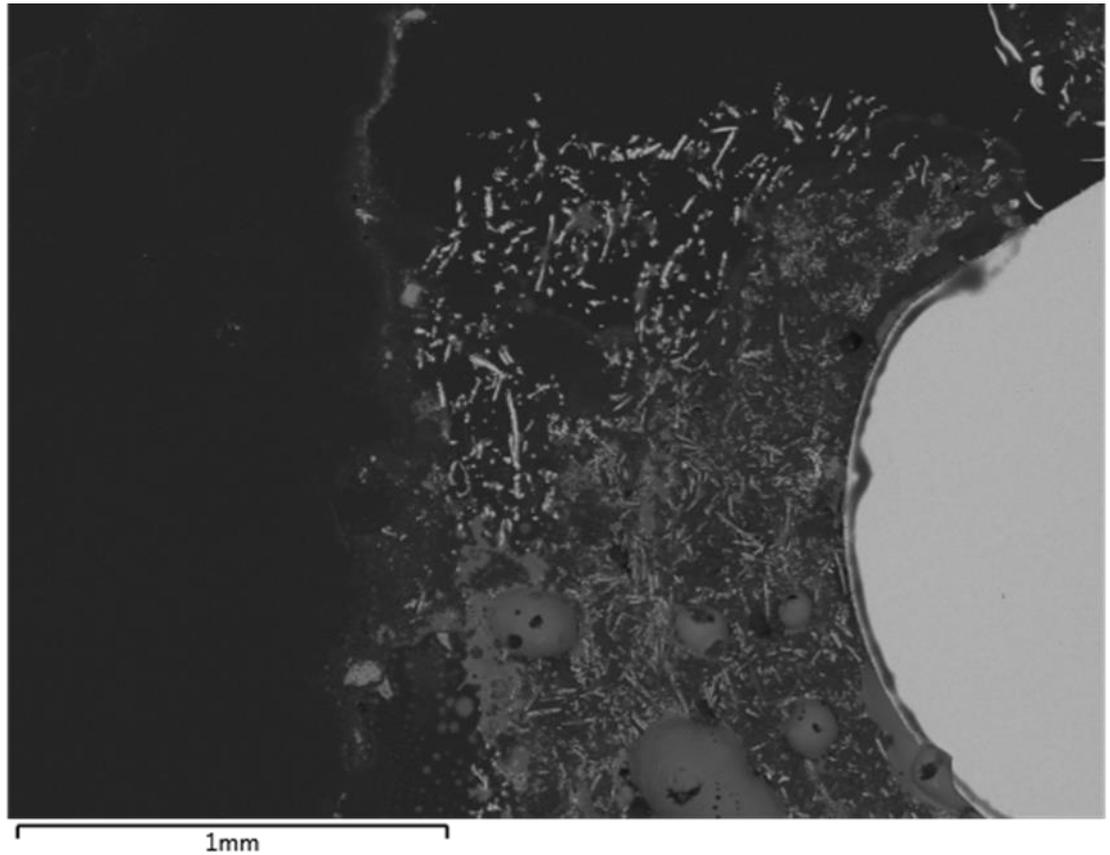

Figure 42. Cathode degradation.
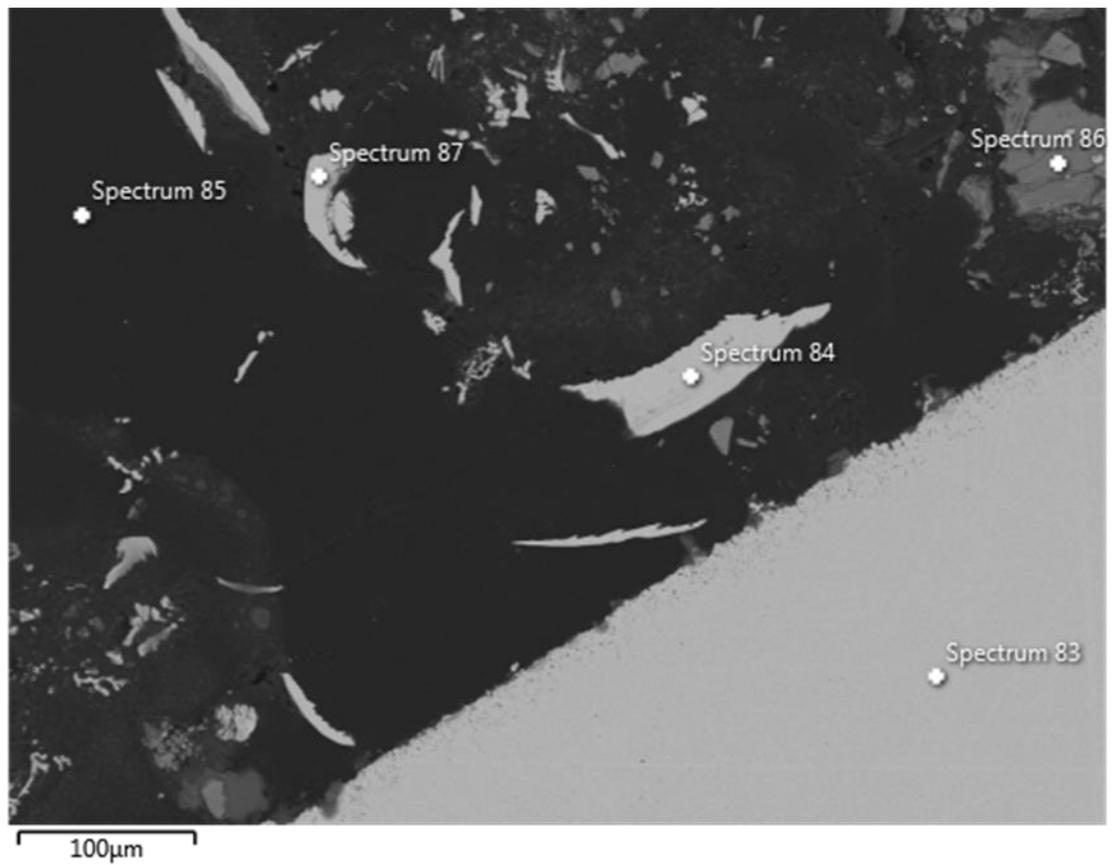
Figure 43. Higher magnification of the cathode degradation (EDS results in Table 23).

Table 23. EDS results for Figure 43.

	Spectrum (wt-%)				
Elements	83	84	85	86	87
O			61.07	35.85	
Mg				1.15	
Al				8.58	
Si	0.82	0.81			0.8
Cl			33.83	0.19	
Ca				0.2	
Ti				0.95	
Cr	20.62	20.4		38.77	20.37
Mn	1.99	2.03			1.96
Fe	66.79	66.92	5.1	14.32	67.66
Ni	9.78	9.84			9.21
Total	100	100	100	100	100

The cathode rod developed some red and green staining on the edges, but this was not visible in FESEM-EDS imagery, the red color may be some hematite and the green color

may have been chromium oxide. The red staining of the cathode rod is shown in Figure 44.

Figure 44. Red staining on the cathode after electrolysis.

The cathode piece with the green staining was also analyzed in FESEM-EDS. Some corrosion caused by the $CaCl_2$ can be seen in Figure 45. The $CaCl_2$ has covered the edge of the cathode and damage can be seen on the edge of the cathode rod. Table 24 shows that spectrum 110 is $CaCl_2$ and spectrum 109 shows that a small amount of $CaCl_2$ is in the corroded cathode edge.
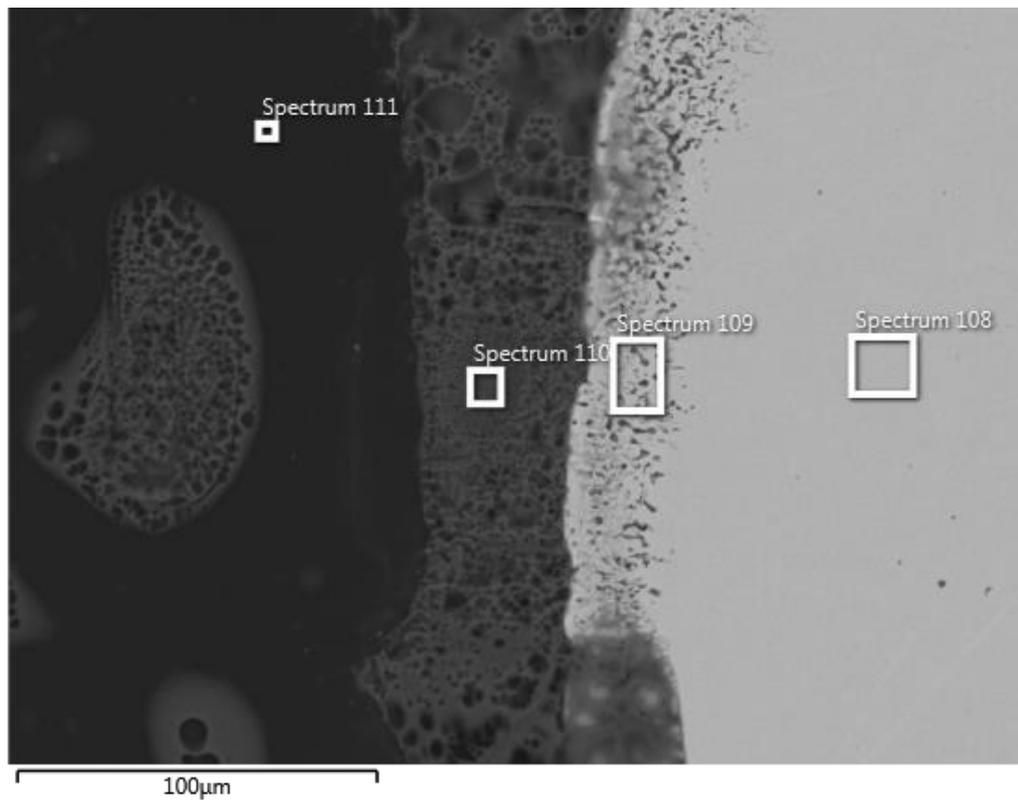
Figure 45. Green cathode corrosion (EDS results in Table 24).

Table 24. EDS results for Figure 45.

	Spectrum (wt-%)			
Elements	108	109	110	111
O		4.61	38.88	79.22
Si	0.83	3.59		
S	0.14	0.18		
Cl		1.44	37.8	20.78
Ca		1.03	22.33	
Cr	20.49	6.07		
Mn	2.17	0.63		
Fe	66.43	65.91	0.99	
Ni	9.95	16.53		
Total	100	100	100	100

Figure 46 shows the anode-crucible assembly after electrolysis. The molten salt has surrounded the anode-crucible area. The molten salt seems to have remained mostly on the edge of the crucible and the graphite anode may have also floated in the molten salt during the experiment.

Figure 46. Crucible and anode bound together by the molten salt.

The anode lost about 5 g of weight in the 1-hour experiment. The starting weight was 216.10 g, and after experiments the measurement was 211.30 g, which corresponds to 2.22% weight loss. This means that some CO_2 emissions were generated during the 1-hour experiment. In further work, it would be relevant to study how much CO_2 is generated relative to the ferrochrome produced. The anode seems to have evenly eroded, as there is no visible deformation. The diameter of the inner circle has increased from 40 mm to 41 mm, which shows that some decomposition of the anode has occurred. The condition of the anode after electrolysis is displayed in Figure 47.

Figure 47. The condition of the anode after the experiments.

4.2 Discussion

The first experiment provided a positive result regarding the reduction of iron and small amounts of chromium in the samples recovered from the suspension but gave also rise to identification on new challenges for further testing of the FFC Cambridge process. The experimental procedure could be improved by sintering the chromite in a controlled lab environment with pressures and temperatures used in other studies. This way the optimal particle size for reduction and strength of the pellets for enduring the electrolytic process remaining with the cathode would be ensured. Alternatively, a basket-type cell configuration could be used, where the reduced pieces of ferrochrome would fall to the basket under the cathode after reduction. CaO could be added to the molten salt to prevent the evaporation of the electrolyte. The crucible size could be larger in height to ensure all pellets have proper contact with the molten electrolyte. Gas vents could be larger to ensure no pressure buildup occurs during experiments, lifting the pellets from the salt. Alternatively, a lower volume of gas flow is an option, if there are cathodes that are rated for lower argon flow.

Multiple issues make the scale-up of the FFC Cambridge process challenging. The reduction process is much slower than with conventional methods, with the shortest time for chromite pellet reduction in literature being about 8 hours (Ge et al. 2015). However, operating with the SOM process could alleviate this problem. The cell size of the FFC Cambridge process has its limits, thus the industrial process should be conducted in a new facility with enough space for multiple cells. The industrial ferrochrome manufacturing processes of today are optimized for the pyrometallurgical processes, thus numerous changes are required to transition into the electrochemical reduction process. One of these issues is the mechanical integrity of the sintered pellets. Also, methods to separate the other reduced and unreduced metals should be considered, if the voltage control of the process is not optimized for the reduction of only chromium and iron. In earlier studies, it has also been difficult to manufacture completely oxygen-free metal, and this may be a big challenge with the industrial standards.

The use of inert anodes is difficult due to changes in the cell voltage values for reduction and there need to be further trials with the possible inert anode alternatives in the chromite reduction process to validate the functionality and practicality of the anodes. It should also be remembered that use of the inert anodes does not make the process

completely CO_2-free; the electricity of the process should come from renewable sources to ensure minimal CO_2 emissions.

The inert atmosphere is made with argon gas flow. Argon is an expensive gas, thus using large quantities in an industrial process seems unfeasible. Trials could be done with other inert gas alternatives, but the safety of the process may be compromised.

This study also was not able to get a definitive answer regarding the amount of energy required for the reduction of pellets. Optimally, the experimental results with full reduction would be available to answer this question, and the cell configuration should be changed for a more accurate analysis of the parameters of electrolysis such as current density. In general, it can be said that this process has good a premise for low-energy operation such as a much lower temperature in comparison with the pyrometallurgical SAF process. The lower temperature also reduces the wear on the materials in the cell, but this benefit is somewhat offset by the corrosive nature of $CaCl_2$.

5 CONCLUSIONS

The FFC Cambridge method has been studied for manufacturing of various metals. For chromite reduction, the most relevant studies available are the reduction of chromite, Cr_2O_3, and Fe_2O_3 using FFC Cambridge electrolysis. However, studies on direct chromite reduction are scarce, as the study by Ge et al. (2015) is the only one thus far.

Numerous different inert anodes have been experimented by several researchers. However, all of these have their drawbacks and benefits, and optimally, the anodes should be tested in their electrolytic environments that are designed for the individual products' processes. Unfortunately, the closest alternative to an inert anode being successfully employed in chromite reduction has been the use of SOM in the Cr_2O_3 reduction. Hopefully, we will have more data on inert anode use in chromite reduction, and this will probably be experimented with in the future.

Cell potential calculations for the different components of the cell and chromite ore were made. The main observations that can be made from these calculations are that the cell potentials are dependent on the partial pressures of CO_2, CO and O_2. Ideally, the partial pressure of CO_2 should be much higher than CO to be able to have a gap between the dissolution potential of CaO and $CaCl_2$. Another observation is related to the reduction of different components in chromite: the vanadium and manganese oxides that are present in the ore are highly likely to reduce with iron and chromium via the FFC Cambridge electrolysis.

The safety of experiments can be ensured, if the experimental apparatus is sealed from air and preheated to ensure minimal partial pressure of oxygen and minimal water contamination. These precautions minimize the risk of hydrolysis and formation of chloride gas. Another risk was the explosive reaction of Cl_2 with hydrocarbons. Hydrocarbon contamination is prevented by using care not to contaminate the furnace or the cell with possible sources of hydrocarbons, such as oils.

The experiments showed that the FFC Cambridge method can reduce Outokumpu's sintered chromite pellets to ferrochrome. However, the experiment's duration was limited, and it is not possible to conclude whether the whole pellet could be reduced via the FFC Cambridge electrolysis. Small, reduced areas however were found in the samples recovered from the suspension.

Numerous challenges related to the scale up the process were identified based on the literature review, experimental design and laboratory experiments conducted:

- voltage limitations of using the inert anodes,
- the corrosive nature of $CaCl_2$,
- the possible corrosion and price of inert anodes,
- the efficiency of the reduction process compared to commercial methods,
- the possible changes that need to be made to the sintering process,
- the necessity to build a large electrolysis hall,
- the separation and prevention of impurities, and
- the costs associated with the use of argon as a protective gas.

The experiments done in this thesis give an insight for the execution of future experimental work. Future experiments could be improved by focusing on analysing the current consumption and gas flow, as they would further improve knowledge of how efficient this process is. If the conventional sintering processes' validity to be used in this process is further studied, the electrolytic cell should include a mesh around the cathode to prevent losing the pellets to the bottom of the crucible. The corrosion of the cathode rod can possibly be prevented by using a kanthal wire as the cathode, as it has been used in past implementations of experimental work. Taller crucibles should be used to make sure every pellet has proper contact with the electrolyte. Overall, the cell configuration should be changed from continuous to batch operation, as the cell assembly had many challenges that could be avoided with a simpler approach.

REFERENCES

Allanore, A. 2014. Features and Challenges of Molten Oxide Electrolytes for Metal Extraction. Journal of the Electrochemical Society, 162 (1), p. E13-E22. doi:10.1149/2.0451501jes

Alzamani, M., Jafarzadeh, K. & Fattah-alhosseini, A., 2021. Development of lanthanum doped Ni10Cu11Fe6Al as a new inert anode in molten salt calcium chloride for titanium oxide electrolysis. Journal of Alloys and Compounds, 876, p. 159997. doi:10.1016/j.jallcom.2021.159997

Barnett, R., Kilby, K. T. & Fray, D. J., 2009. Reduction of Tantalum Pentoxide Using Graphite and Tin-Oxide-Based Anodes *via* the FFC-Cambridge Process. Metallurgical and Materials Transactions. B, Process Metallurgy and Materials Processing Science, 40 (2), p. 150-157. doi:10.1007/s11663-008-9219-6

Burheim, O. & Haarberg, G. M., 2010. Effects of inert anodes in the FFC Cambridge reduction of hematite. Institution of Mining and Metallurgy. Transactions. Section C: Mineral Processing and Extractive Metallurgy, 119 (2), p. 77-81. doi:10.1179/037195510X12665949176454

Chen, G. Z., 2015. The FFC Cambridge process and its relevance to valorisation of ilmenite and titanium-rich slag. Institution of Mining and Metallurgy. Transactions. Section C: Mineral Processing and Extractive Metallurgy, 124 (2), p. 96-105. doi:10.1179/1743285514Y.0000000073

Chen, G. Z., 2020. Interactions of molten salts with cathode products in the FFC Cambridge Process. International Journal of Minerals, Metallurgy and Materials, 27 (12), p. 1572-1587. doi:10.1007/s12613-020-2202-1

Chen, G. Z., Gordo, E. & Fray, D. J., 2004. Direct electrolytic preparation of chromium powder. Metallurgical and Materials Transactions. B, Process Metallurgy and Materials Processing Science, 35 (2), p. 223-233. doi:10.1007/s11663-004-0024-6

Chen, G. Z. & Fray, D. J., 2006. A morphological study of the FFC chromium and titanium powders. Institution of Mining and Metallurgy. Transactions. Section C: Mineral Processing and Extractive Metallurgy, 115 (1), p. 49-54. doi:10.1179/174328506X91365

Ding, W., Bonk, A. & Bauer, T., 2018. Molten chloride salts for next generation CSP plants: Selection of promising chloride salts & study on corrosion of alloys in molten chloride salts. AIP Conference Proceedings, 2126 (1) p. 20014. doi:10.1063/1.5117729

Erkkilä, P., 2004. Trends and challenges in the stainless steel industry. Ironmaking & Steelmaking, 31 (4), p. 277-284. doi:10.1179/030192304225018280

Esmaily, M., Mortazavi, A. N., Birbilis, N. & Allanore, A., 2020. Oxidation and electrical properties of chromium–iron alloys in a corrosive molten electrolyte environment. Scientific Reports, 10 (1), p. 14833. doi:10.1038/s41598-020-71903-0

Espinha Marques, J., Marques, J. M., Carvalho, A., Carreira, P. M., Moura, R. & Mansilha, C., 2019. Groundwater resources in a Mediterranean mountainous region: Environmental impact of road de-icing. Sustainable Water Resources Management, 5 (1), p. 305-317. doi:10.1007/s40899-017-0170-z

Fenn, A.J. & Cooley, G. & Fray, D.J. & Smith, L., 2004. Exploiting the FFC Cambridge process. Advanced Materials and Processes, 162 (2) p. 51-53.

Fray, D. J., Chen, G. Z. & Farthing, T. W., 2000. Direct electrochemical reduction of titanium dioxide to titanium in molten calcium chloride. Nature (London), 407 (6802), p. 361-364. doi:10.1038/35030069

Ge, X., Jin, S., Zhang, M., Wang, X. & Seetharaman, S., 2015. Synthesis of chromium and ferrochromium alloy in molten salts by the electro-reduction method. Journal of Mining and Metallurgy. Section B, Metallurgy, 51 (2), p. 185-191. doi:10.2298/JMMB141222022G

Gordo, E., Chen, G. Z. & Fray, D. J., 2004. Toward optimisation of electrolytic reduction of solid chromium oxide to chromium powder in molten chloride salts. Electrochimica Acta, 49 (13), p. 2195-2208. doi:10.1016/j.electacta.2003.12.045

Guoming, L. Dihua, W., Chen, Z., 2009. Direct Reduction of Solid Fe_2O_3 in Molten $CaCl_2$ by Potentially Green Process. Journal of Materials Science & Technology, 25 (6), p. 767-771.

Gynther L. & Kiuru, T., 2020. Energy Efficiency of Metals Production Industry in Finland [online document]. Helsinki: Motiva. Available from: https://www.motiva.fi/files/18167/Energy_Efficiency_of_Metals_Production_Industry_in_Finland_-_December_2020.pdf [Accessed 10.9.2022]. 39 p.

Habashi, F. (ed.), 1997. Handbook of Extractive Metallurgy. Weinhein: Wiley-VCH, 2379 p. ISBN: 3-527-28792-2

Hagen, E., Rian, G., Rosenkilde, C., Vigeland, B.E., Lorentsen, O. A., 2007. Method and Means for Metal Production in Chloride Melts. World Intellectual Property Organization, International Bureau. Patent no. WO 2007/094681 A1. Available from: https://patents.google.com/patent/WO2007094681A1/en [Accessed 11.5.2022].

Hamuyuni, J., Johto, H., Haimi, T., Bunjaku, A., Mäkelä, P., Närhi, L. and Lindgren, M., 2021. Evaluating the Carbon Footprint of Ferrochrome Production Technologies using HSC-SIM and OpenLCA Software Packages. Proceedings of the 16th International Ferro-Alloys Congress (INFACON XVI) 2021

Heikkilä, A. M., Pussinen, J. H., Mattila, O. J. & Fabritius, T. M. J., 2015. About Electrical Properties of Chromite Pellets - Effect of Reduction Degree. Steel Research International, 86 (2), p. 121-128. doi:10.1002/srin.201400023

International Stainless Steel Forum, 2022. The Stainless Steel Family [online document]. Belgium: worldstainless. Available from: https://www.worldstainless.org/Files/issf/non-image-files/PDF/TheStainlessSteelFamily.pdf [Accessed 5.9.2022].

Jiang, K., Hu, X., Ma, M., Wang, D., Qiu, G., Jin, X. & Chen, G. Z., 2006. "Perovskitization"-Assisted Electrochemical Reduction of Solid TiO_2 in Molten $CaCl_2$. Angewandte Chemie (International ed.), 45 (3), p. 428-432. doi:10.1002/anie.200502318

Jiao, H., Tian, D., Tu, J. & Jiao, S., 2018. Production of Ti-Fe alloys via molten oxide electrolysis at a liquid iron cathode. RSC Advances, 8 (31), p. 17575-17581. doi:10.1039/C8RA01646A

Jiao, S., Jiao, H., Song, W., Wang, M. & Tu, J., 2020. A review on liquid metals as cathodes for molten salt/oxide electrolysis. International Journal of Minerals, Metallurgy and Materials, 27 (12), p. 1588-1598. doi:10.1007/s12613-020-1971-x

Jiao, S. & Fray, D. J. 2010. Development of an Inert Anode for Electrowinning in Calcium Chloride–Calcium Oxide Melts. Metallurgical and Materials Transactions. B, Process Metallurgy and Materials Processing Science, 41 (1), p. 74-79. doi:10.1007/s11663-009-9281-8

Kim, H., Paramore, J. D., Allanore, A. & Sadoway, D. R., 2019. Stability of Iridium Anode in Molten Oxide Electrolysis for Ironmaking: Influence of Slag Basicity. ECS Transactions, 33 (7), p. 219-230. doi:10.1149/1.3484779

King H. M., 2022. Home, Minerals, Chromite [online document]. Unknown: Geology.com Available from: https://geology.com/minerals/chromite.shtml [Accessed 5.11.2022].

Kvande, H & Vidal, J. C., 2019. Molten salt electrolysis. In: Kawatra, S.K.,Young, C.A., Dunne R.C. (eds). SME Mineral Processing and Extractive Metallurgy Handbook Englewood, Colorado: Society for Mining, Metallurgy, and Exploration, Inc, 2019. ISBN: 9780873353854.

Li C.-J., Li P., Wang K., Molina E. E., 2014. Survey of Properties of Key Single and Mixture Halide Salts for Potential Application as High Temperature Heat Transfer Fluids for Concentrated Solar Thermal Power Systems[J]. AIMS Energy, 2014, 2 (2): p. 133-157. doi: 10.3934/energy.2014.2.133

Liu, Z., Zhang, H., Pei, L., Shi, Y., Cai, Z., Xu, H. & Zhang, Y., 2018. Direct electrolytic preparation of chromium metal in CaCl2–NaCl eutectic salt. Transactions of Nonferrous Metals Society of China, 28 (2), p. 376-384. doi:10.1016/S1003-6326(18)64671-0

Martin, A., Poignet, J. C., Fouletier, J., Allibert, M., Lambertin, D. & Bourgès, G., 2009. Yttria-stabilized zirconia as membrane material for electrolytic deoxidation of CaO–CaCl$_2$ melts. Journal of Applied Electrochemistry, 40 (3), p. 533-542. doi:10.1007/s10800-009-0025-x

Metallinjalostajat, 2014. Teräskirja. 9th edition. Helsinki: Metallinjalostajat, 112. p. ISBN 978-952-238-120-0

Merck, 2022. Home, Search results, Tin(IV) oxide [online document]. Germany: Merck KGaA   Available   from: https://www.sigmaaldrich.com/FI/en/substance/tinivoxide1507118282105   [Accessed 12.12.2022]

Meurisse, A., Lomax, B., Selmeci, Á., Conti, M., Lindner, R., Makaya, A., Carpenter, J., 2022. Lower temperature electrochemical reduction of lunar regolith simulants in molten salts. Planetary and Space Science, 211, p. 105408. doi:10.1016/j.pss.2021.105408

Mohandas, K. S., 2013. Direct electrochemical conversion of metal oxides to metal by molten salt electrolysis: A review. Institution of Mining and Metallurgy. Transactions. Section C: Mineral Processing and Extractive Metallurgy, 122 (4), p. 195-212. doi:10.1179/0371955313Z.00000000069

Mohandas, K.S., Shakila, L., Sanil, N., Sri, D., Vishnu, D., Nagarajan, K., 2011. Galvanostatic Studies on the Electro-Deoxidation of Solid Titanium Dioxide in Molten Calcium Chloride. In: Kongoli, F. (ed.) Fray International Symposium Metals and Materials Processing in a Clean Environment Volume 3: Molten Salts & Ionic Liquids 2011. doi:10.13140/2.1.1824.0642

Monex, 2022. Platinum prices, MONEX Live Platinum Spot Prices [online document]. Unknown: Monex Deposit Company Available from: https://www.monex.com/platinum-prices/ [Accessed 28.4.2022]

Outokumpu, 2013. Handbook of Stainless Steels [online document]. Espoo: Outokumpu Oyj. Available from: http://www.steel-stainless.org/media/1546/outokumpu-stainless-steel-handbook.pdf [Accessed 27.3.2022]. 92p.

Outokumpu, 2020. Expertise, Comparing carbon footprints how to avoid the pitfalls [online document]. Unknown: Outokumpu Oyj. Available from: https://www.outokumpu.com/fi-fi/expertise/2020/comparing-carbon-footprints-how-to-avoid-the-pitfalls [Accessed 4.3.2022].

Outokumpu, 2022a. About Outokumpu, Ferrochrome [online document]. Unknown: Outokumpu Oyj. Available from: https://www.outokumpu.com/fi-fi/about-outokumpu/organization/ferrochrome [Accessed 4.3.2022].

Outokumpu, 2022b. Expertise, The effects of alloying elements [online document]. Unknown: Outokumpu Oyj. Available from: https://www.outokumpu.com/en/expertise/stainless-basics/the-effects-of-alloying-elements [Accessed 4.3.2022].

Riekkola-Vanhanen, M., 1999. Finnish expert report on best available techniques in ferrochromium production [online document]. Helsinki: Oy Edita Ab. Available from: https://helda.helsinki.fi/bitstream/handle/10138/40531/FE_314.pdf?sequence=1 [Accessed: 20.5.2022]. 49 p.

Rumble, J. R., 2022. Physical constants of inorganic compounds. In: Rumble, J. R. (ed.) CRC Handbook of Chemistry and Physics. 103rd Edition (Internet Version 2022) Boca Raton: CRC Press/Taylor & Francis. ISBN: 978-1032121710

Schwandt, C. & Fray, D. J., 2007. The Electrochemical Reduction of Chromium Sesquioxide in Molten Calcium Chloride under Cathodic Potential Control. Zeitschrift für Naturforschung. A, A Journal of Physical Sciences, 62 (10), p. 655-670. doi:10.1515/zna-2007-10-1115

Schwandt, C., 2013. Understanding the electro-deoxidation of titanium dioxide to titanium metal via the FFC-Cambridge process. Institution of Mining and Metallurgy. Transactions. Section C: Mineral Processing and Extractive Metallurgy, 122 (4), p. 213-218. doi:10.1179/0371955313Z.00000000071

Scott, K., 2019. Introduction to Electrolysis, Electrolysers and Hydrogen Production. In: Scott, K. (ed.) Electrochemical Methods for Hydrogen Production. Newcastle: Royal

Society of Chemistry, p. 1-27. ISBN: 978-1-78801-604-9 doi:10.1039/9781788016049-00001

Shurov, N. I., Khramov, A. P., Zaikov, Y. P., Kovrov, V. A. & Suzdal'tsev, A. V., 2015. Reduction mechanism of oxides in calcium chloride melts. Russian Journal of Non-Ferrous Metals, 56 (3), p. 267-271. doi:10.3103/S1067821215030207

Stibbs, J. & Pan, S., 2022. Insights, Graphite electrode prices in China edged upward on rising needle coke costs [online document]. Unknown: Fastmarkets. Available from: https://www.fastmarkets.com/insights/graphite-electrode-prices-in-china-edged-upward-on-rising-needle-coke-costs [Accessed 14.5.2022].

Suzuki, R.O., Natsui, S., Kikuchi T., 2020. OS process: calciothermic reduction of TiO_2 via CaO electrolysis in molten $CaCl_2$. In: Fang, Z.Z., Froes, F.H., Zhang, Y. (eds.) Extractive Metallurgy of Titanium: conventional and recent advances in extraction and production of titanium metal. Amsterdam: Elsevier 2020, p. 287-313. ISBN: 9780128172001 doi:10.1016/B978-0-12-817200-1.00012-0

The National Center for Biotechnology Information, 2022a. Compound summary: Tin(IV) oxide [online document]. Bethesda: The National Center for Biotechnology Information. Available from: https://pubchem.ncbi.nlm.nih.gov/compound/29011 [Accessed 10.12.2022].

The National Center for Biotechnology Information, 2022b. Periodic table, Element summary: Platinum [online document]. Bethesda: The National Center for Biotechnology Information. Available from: https://pubchem.ncbi.nlm.nih.gov/element/Platinum [Accessed 10.12.2022].

Tokai Carbon, 2022. Top, Business, Graphite electrodes [online document]. Tokyo: Tokai Carbon. Available from: https://www.tokaicarbon.co.jp/en/products/graphite/ [Accessed 14.5.2022].

Työterveyslaitos, 2022. OVA-ohjeet, Kloori [online document]. Unknown: Työterveyslaitos. Available from: https://www.ttl.fi/ova/kloori [Accessed 6.12.2022].

Umicore, 2022. Precious Metals Management, Prices, Ruthenium price [online document]. Unknown: Umicore. Available from: https://pmm.umicore.com/en/prices/ruthenium/ [Accessed 6.12.2022].

Villars, P., 2016a. $CaRuO_3$ Crystal Structure [online database]. Heidelberg: Springer Nature Switzerland AG. Available from: https://materials.springer.com/isp/crystallographic/docs/sd_0560998 [Accessed 6.12.2022].

Villars, P., 2016b. $NiFe_2O_4$ Crystal Structure [online database]. Heidelberg: Springer Nature Switzerland AG. Available from: https://materials.springer.com/isp/crystallographic/docs/sd_0551821 [Accessed 6.12.2022].

Wang, D. & Xiao, W., 2013. Inert Anode Development for High-Temperature Molten Salts. In: Lantelme, F. & Groult, H. (Eds.) Molten Salts Chemistry From Lab to Applications. Edition 1. Amsterdam: Elsevier 2013, p. 171-186. ISBN: 9780124017221 doi:10.1016/B978-0-12-398538-5.00009-3.

Wang, B., Chen, C., Li, J., Wang, L., Lan, Y. & Wang, S., 2020. Solid oxide membrane-assisted electrolytic reduction of Cr_2O_3 in molten $CaCl_2$. International Journal of Minerals, Metallurgy and Materials, 27 (12), p. 1626-1634. doi:10.1007/s12613-020-2141-x

Wiencke, J., Lavelaine, H., Panteix, P., Petitjean, C. & Rapin, C., 2018. Electrolysis of iron in a molten oxide electrolyte. Journal of Applied Electrochemistry, 48 (1), p. 115-126. doi:10.1007/s10800-017-1143-5

Yan, Y. & Fray, D., 2010. Molten salt electrolysis for sustainable metals extraction and materials processing a review. In: Kuai, S. & Meng J. (Eds.) Electrolysis: Theory, Types and Applications. New York: Nova Science Publishers, Inc., p. 255-302. ISBN: 978-1-60876-619-2

Yvonne, 2020. Home, Question, Graphite Electrode, Graphite electrode dia and graphite electrode melting point [online document]. Shanghai: Dan Carbon Company Limited.

Available from: https://www.dancarbon.com/q/graphite-electrode/163.html [Accessed 24.4.2022].

Zhang, X., Jiao, K., Zhang, J. & Guo, Z., 2021. A review on low carbon emissions projects of steel industry in the World. Journal of Cleaner Production, 306, p. 127259. doi:10.1016/j.jclepro.2021.127259